# JCI The Journal of Clinical Investigation

# High 4E-BP-1 expression associates with chromosome 8 gain and CDK4/6 sensitivity in Ewing Sarcoma

Cornelius M. Funk, Anna C. Ehlers, Martin F. Orth, Karim Aljakouch, Jing Li, Tilman L.B. Hoelting, Rainer Will, Florian H. Geyer, A. Katharina Ceranski, Franziska Willis, Endrit Vinca, Shunya Ohmura, Roland Imle, Jana Siebenlist, Angelina Yershova, Maximilian M.L. Knott, Felina Zahnow, Ana Sastre, Javier Alonso, Felix Sahm, Heike Peterziel, Anna Loboda, Martin Schneider, Ana Banito, Gabriel Leprivier, Wolfgang Hartmann, Uta Dirksen, Olaf Witt, Ina Oehme, Stefan M. Pfister, Laura Romero-Pérez, Jeroen Krijgsveld, Florencia Cidre-Aranaz, Thomas G.P. Grünewald, Julian Musa

J Clin Invest. 2025. https://doi.org/10.1172/JCI187627.

Research In-Press Preview Genetics Oncology

Chromosome 8 (chr8) gains are common in cancer, but their contribution to tumor heterogeneity is largely unexplored. Ewing sarcoma (EwS) is defined by *FET::ETS* fusions with few other recurrent mutations to explain clinical diversity. In EwS, chr8 gains are the second most frequent alteration, making it an ideal model to study their relevance in an otherwise silent genomic context. We report that chr8 gain-driven expression patterns correlate with poor overall survival of EwS patients. This effect is mainly mediated by increased expression of the translation initiation factor binding protein 4E-BP1, encoded by *EIF4EBP1* on chr8. Among all chr8-encoded genes, *EIF4EBP1* expression showed the strongest association with poor survival and correlated with chr8 gains in EwS tumors. Similar findings emerged across multiple TCGA cancer entities. Multi-omics profiling revealed that 4E-BP1 orchestrates a pro-proliferative proteomic network. Silencing 4E-BP1 reduced proliferation, clonogenicity, spheroidal growth in vitro, and tumor growth in vivo. Drug screens demonstrated that high 4E-BP1 expression sensitizes EwS to pharmacological CDK4/6-inhibition. Chr8 gains and elevated 4E-BP1 emerge as prognostic biomarkers in EwS, with poor outcomes driven by 4E-BP1-mediated proproliferative networks that sensitize tumors to CDK4/6 inhibitors. Testing for chr8 gains may enhance risk stratification and therapy in EwS and other cancers.

#### Find the latest version:



#### High 4E-BP-1 expression associates with chromosome 8 gain and CDK4/6 sensitivity in **Ewing Sarcoma**

Cornelius M. Funk<sup>1,2,3,\*</sup>, Anna C. Ehlers<sup>1,2,3,\*</sup>, Martin F. Orth<sup>4</sup>, Karim Aljakouch<sup>5,6</sup>, Jing Li<sup>1,2,3</sup>, Tilman L. B. Hölting<sup>1,2,3,7</sup>, Rainer Will<sup>8</sup>, Florian H. Geyer<sup>1,2,3</sup>, A. Katharina Ceranski<sup>1,2,3</sup>, Franziska Willis<sup>9,10</sup>, Endrit Vinca<sup>1,2,3</sup>, Shunya Ohmura<sup>1,2,3</sup>, Roland Imle<sup>2,3,11,12,13</sup>, Jana Siebenlist<sup>1,2,3</sup>, Angelina Yershova<sup>1,2,3</sup>, Maximilian M. L. Knott<sup>14,15</sup>, Felina Zahnow<sup>1,2,3</sup>, Ana Sastre<sup>16</sup>, Javier Alonso<sup>17,18</sup>, Felix Sahm<sup>19,20</sup>, Heike Peterziel<sup>2,3,21</sup>, Anna Loboda<sup>2,3,21,22</sup>, Martin Schneider<sup>9,10</sup>, Ana Banito<sup>2,3,11</sup>, Gabriel Leprivier<sup>23</sup>, Wolfgang Hartmann<sup>24</sup>, Uta Dirksen<sup>25</sup>, Olaf Witt<sup>2,3,21,26</sup>, Ina Oehme<sup>2,3,26</sup>, Stefan M. Pfister<sup>2,3,21,27</sup>, Laura Romero-Pérez<sup>1,2,3,28,29</sup>, Jeroen Krijgsveld<sup>5,22</sup>, Florencia Cidre-Aranaz<sup>1,2,3</sup>, Thomas G. P. Grünewald<sup>1,2,3,4,30,\*,§</sup>, Julian Musa<sup>1,2,3,9,10</sup>\*

- \* C.M.F. and A.C.E. share first authorship
- \* T.G.P.G. and J.M. share senior authorship

#### Author affiliations:

- 1 German Cancer Research Center (DKFZ) Heidelberg, Division of Translational Pediatric Sarcoma Research, Germany
- 2 Hopp Children's Cancer Center Heidelberg (KiTZ), Heidelberg, Germany
  3 National Center for Tumor Diseases (NCT), NCT Heidelberg, a partnership between DKFZ and Heidelberg University Hospital, Germany
- 4 Max-Eder Research Group for Pediatric Sarcoma Biology, Institute of Pathology, Faculty of Medicine, LMU Munich, Munich, Germany
- 5 German Cancer Research Center (DKFZ) Heidelberg, Division of Proteomics of Stem Cells and Cancer, Germany
- 6 Medical Faculty, Heidelberg University, Heidelberg, Germany
- 7 Department of Medical Oncology, National Centre for Tumor Diseases, Heidelberg, Germany
- 8 Cellular Tools Core Facility, German Cancer Research Center (DKFZ), German Cancer Consortium (DKTK), Heidelberg, Germany
- 9 Department of General, Visceral, and Transplantation Surgery, University Hospital Heidelberg, Heidelberg, Germany
- 10 Department of General, Visceral, Thoracic, and Transplantation Surgery, University Hospital Giessen and Marburg, Giessen, Germany
- 11 Soft-Tissue Sarcoma Junior Research Group, German Cancer Research Center (DKFZ), Heidelberg, Germany
- 12 Division of Pediatric Surgery, University Hospital Heidelberg, Heidelberg, Germany
- 13 Faculty of Biosciences, Heidelberg University, Heidelberg, Germany
- 14 Institute of Pathology, Faculty of Medicine, LMU Munich, Munich, Germany
- 15 Present address: Department of Neurobiology, Faculty of Life Sciences & Sagol School of Neuroscience, Tel Aviv University, Tel Aviv, Israel
- 16 Unidad Hemato-oncología Pediátrica, Hospital Infantil Universitario La Paz, Madrid, Spain
- 17 Pediatric Solid Tumour Laboratory, Institute of Rare Diseases Research (IIER), Institute de Salud Carlos III, Madrid, Spain
- 18 Centro de Investigación Biomédica en Red de Enfermedades Raras, Instituto de Salud Carlos III (CB06/07/1009; CIBERER-ISCIII), Madrid, Spain
- 19 German Cancer Research Center (DKFZ) Heidelberg, Clinical Cooperation Unit Neuropathology, Germany
- 20 Department of Neuropathology, University Hospital Heidelberg, Heidelberg, Germany
- 21 Department of Pediatric Oncology, Hematology, Immunology and Pulmonology, Heidelberg University Hospital, Heidelberg, Germany
- 22 Faculty of Biosciences, Heidelberg University, Heidelberg, Germany
- 23 Institute of Neuropathology, University Hospital Düsseldorf, Medical Faculty, Heinrich Heine University, Düsseldorf, Germany
- 24 Division of Translational Pathology, Gerhard-Domagk-Institute of Pathology, University Hospital of Münster, Münster, Germany
  25 Pediatrics III, West German Cancer Center, German Cancer Consortium site Essen, National Cancer Center (NCT) site Essen, University Hospital of Essen, Essen,
- 26 German Cancer Research Center (DKFZ) Heidelberg, Clinical Cooperation Unit Pediatric Oncology, Germany
- 27 German Cancer Research Center (DKFZ) Heidelberg, Division of Pediatric Neurooncology, Germany
- 28 Division of Molecular Pathology of Sarcomas, Institute of Biomedicine of Sevilla (IBiS), Virgen del Rocio University Hospital/CSIC/University of Sevilla/CIBERONC,
- 29 Department of Normal and Pathological Cytology and Histology, School of Medicine, University of Seville, Spain
- 30 Institute of Pathology, Heidelberg University Hospital, Heidelberg, Germany

#### § Address for correspondence

Thomas G. P. Grünewald, MD, PhD

Division Head, Division of Translational Pediatric Sarcoma Research (B410)

German Cancer Research Center (DKFZ) & Hopp-Children's Cancer Center (KiTZ)

Im Neuenheimer Feld 280, 69210 Heidelberg, Germany

Phone +49-6221-42-3718

Email t.gruenewald@kitz-heidelberg.de

**Word count:** 11.835

**Display items:** 4 Figures, 4 Supplementary Figures, 18 Supplementary Tables

**Running title:** Chromosome 8 gain sensitizing for CDK4/6 inhibition

Chromosome 8 gain, EIF4EBP1, 4E-BP1, Ewing sarcoma, CDK4/6 inhibitor, **Key words:** 

Palbociclib, Ribociclib

#### **ABSTRACT**

Chromosome 8 (chr8) gains are common in cancer, but their contribution to tumor heterogeneity is largely unexplored. Ewing sarcoma (EwS) is defined by *FET::ETS* fusions with few other recurrent mutations to explain clinical diversity. In EwS, chr8 gains are the second most frequent alteration, making it an ideal model to study their relevance in an otherwise silent genomic context.

We report that chr8 gain-driven expression patterns correlate with poor overall survival of EwS patients. This effect is mainly mediated by increased expression of the translation initiation factor binding protein 4E-BP1, encoded by *EIF4EBP1* on chr8. Among all chr8-encoded genes, *EIF4EBP1* expression showed the strongest association with poor survival and correlated with chr8 gains in EwS tumors. Similar findings emerged across multiple TCGA cancer entities. Multi-omics profiling revealed that 4E-BP1 orchestrates a pro-proliferative proteomic network. Silencing 4E-BP1 reduced proliferation, clonogenicity, spheroidal growth *in vitro*, and tumor growth *in vivo*. Drug screens demonstrated that high 4E-BP1 expression sensitizes EwS to pharmacological CDK4/6-inhibition.

Chr8 gains and elevated 4E-BP1 emerge as prognostic biomarkers in EwS, with poor outcomes driven by 4E-BP1-mediated pro-proliferative networks that sensitize tumors to CDK4/6 inhibitors. Testing for chr8 gains may enhance risk stratification and therapy in EwS and other cancers.

#### **INTRODUCTION**

Aneuploidy is common in cancer cells and plays an important functional role in their pathophysiology (1–3). Copy number alterations of chr8, especially chr8 gains, are observed in numerous cancer entities, including EwS, acute/chronic myeloid leukemia, gastric cancer, myxoid liposarcoma, pediatric undifferentiated sarcoma, clear cell sarcoma, and malignant peripheral nerve sheath tumors (2, 4–11). However, the functional and clinical role of chr8 gains remains to be clarified. In the context of precision oncology, understanding the role of specific chromosomal gains and losses as one major source of inter-tumor heterogeneity is important for the development of novel personalized diagnostic and therapeutic approaches.

EwS is a malignant bone- and soft tissue-associated tumor, primarily occurring in children, adolescents, and young adults (12). It is characterized by a low number of recurrent somatic mutations and is driven by chromosomal translocations generating pathognomonic *FET::ETS* fusions (consisting of members from the *FUS/EWS/TAF15* (FET) gene family and the E26 Transformation-Specific (ETS) gene family) with *Ewing sarcoma breakpoint region 1::Friend leukemia integration 1 (EWSR1::FLI1)* being the most common (present in 85% of cases), encoding aberrant chimeric transcription factors (12). Genetic variants in polymorphic enhancer-like DNA binding sites of EWSR1::FLI1 were shown to account for inter-individual heterogeneity in EwS susceptibility, tumor growth, clinical course, and treatment response (13–15). Secondary somatic mutations in *STAG2* and *TP53* occur in approximately 20 and 5% of EwS patients (16–18), respectively. However, little is known about other even more common recurrent alterations, such as chromosomal gains and/or losses, and their impact on inter-individual tumor heterogeneity.

Chr8 gain is present in approximately 50% of EwS cases, often in form of chr8 trisomy, making it the second most frequently observed recurrent somatic alteration in EwS following *FET::ETS* fusions (16–22). Previous studies focused solely on specific correlations regarding the role of (partial) chr8 gains in EwS (16–19, 21, 23–28), and suggested that chr8 gains may be an early event in EwS tumorigenesis (29). However, the precise functional and clinical impact of whole chr8 gains

in EwS remains unclear. EwS serves as an ideal model to investigate the role of chr8 gain in cancer, given that EwS exhibit a 'silent' genome, where chr8 gains occur in an oligomutated genomic context (12).

Therefore, the present study aimed to investigate the possible association between whole chr8 gains and tumor progression in the EwS model and to identify the most clinically relevant genes located on chr8 that may functionally contribute to inter-individual variability in patient outcomes. Following an integrative functional genomics approach, we have identified the eukaryotic translation initiation factor 4E binding protein 1 (EIF4EBP1, alias 4E-BP1) as the most promising chr8 candidate gene. It is outstandingly associated with unfavorable EwS patient outcome compared to all other captured genes located on chr8 and even across the entire EwS transcriptome. 4E-BP1 functions downstream of its inactivating kinase complex, mTORC1 (mammalian target of rapamycin complex 1), and is a key effector of the mTORC1 signaling pathway (30, 31). 4E-BP1 belongs to a family of eIF4E-binding proteins that enable mTORC1 to adjust mRNA translation rates in response to various stimuli by modulating the assembly of the 48S translation initiation complex (30, 32–34). 4E-BP1 essentially blocks overall cap-dependent mRNA translation rates, but as well exerts selectivity in promoting and inhibiting translation of specific transcripts (30, 34–42). However, its precise and maybe dynamic role in tumor initiation and/or progression is still ambiguous and a current matter of debate since tumor suppressing (43-45) and tumor promoting (30, 37, 42, 45, 46) roles of 4E-BP1 have been described depending on the cancer entity and cellular context (30, 37, 42, 45, 46).

In the current study, we demonstrate that overexpression of *EIF4EBP1* is mediated by chr8 gain in primary EwS tumors. Furthermore, its RNAi-mediated knockdown in cell line models reduces EwS growth *in vitro* and *in vivo*, by influencing a pro-proliferative proteomic network. Thus, we establish an association between chr8 gain and tumor progression, mediated by 4E-BP1 in EwS. Drug screens and drug sensitivity assays *in vitro* and *in vivo* revealed that high 4E-BP1 expression sensitizes cells to targeted CDK4/6 inhibitor treatment with the FDA-approved drugs Palbociclib and Ribociclib.

This discovery offers a therapeutic strategy for tumors with chr8 amplification and 4E-BP1 overexpression.

#### **RESULTS**

## Chromosome 8 gain drives overexpression of the clinically relevant translational regulator 4E-

**BP1 in EwS** 

To gain initial insights into whether chr8 gain mediates poor patient outcomes in EwS, we analyzed a cohort of 196 EwS samples for which matched microarray gene expression data and clinical data were available (henceforth referred to as 'Cohort 1'). We used a chr8 gene expression signature as a surrogate model for factual genomic chr8 gain and performed a single-sample Gene Set Enrichment Analysis (ssGSEA) followed by hierarchical clustering (Figure 1a) (47, 48). Each patient was stratified to either a high or low chr8 gene expression signature group based on hierarchical clustering of sample-specific ssGSEA enrichment scores for the chromosome 8 gene set (Figure 1a). To validate our approach, we first identified the differentially expressed genes (DEGs) between the inferred chr8 high and low clusters. We then performed a Position Related Data Analysis (PREDA), which identifies chromosomal location of the respective DEGs and maps them to the respective chromosomal positions (49, 50). PREDA analysis demonstrated that the vast majority of DEGs map to chr8 validating the inferred chr8 signature (Supplementary Figure 1a). Secondly, we applied our approach to RNA-sequencing data from an independent cohort of 100 EwS tumors (henceforth referred to as 'Cohort 2') and compared the chr8 signature enrichment clustering with matched factual chr8 copy-number variation (CNV) status (inferred from DNA methylation arrays). This analysis showed that clustering based on the chr8 gene expression signature enrichment accurately indicates the presence of chr8 gain (Supplementary Figure 1b). Kaplan-Meier analysis in Cohort 1 revealed that a high chr8 gene expression signature was associated with shorter overall EwS patient survival (P=0.0137, Figure 1b). Strikingly, this association remained significant (P=0.0309, Figure 1b) even when only considering patients with

localized disease (i.e., without evidence for metastasis at diagnosis), indicating that chr8 gain is functionally involved in mediating an unfavorable disease phenotype. In support of this hypothesis, it is intriguing that while chr8 gain is only found in approximately 50% of primary tumors, around 80% of EwS cell lines, which are expected to be derived from highly aggressive tumor clones, exhibit chr8 gains (mostly trisomies) (16–19, 21, 24–28). Since previous studies have reported that chr8 gains can co-occur with other recurrent chromosomal gains and losses that may have an effect on patient overall survival (16–18, 27), such as chr1q gains, chr12 gains, and 16q loss, we reanalyzed our Cohort 1 only focusing on those patients that showed an exclusive predicted chr8 gain versus those harboring none of the above-mentioned CNVs to rule out possible confounding other gains and losses. As shown in **Figure 1c**, this yielded even a better patient-stratification regarding overall survival in both localized disease and the entire sub-cohort (*P*=0.0115 and *P*=0.0033, respectively). Together, these findings suggest that genes located on chr8 contribute to aggressive cellular behavior and disease progression in EwS.

Previous reports suggested that *MYC* located on chr8 may mediate the effect of chr8 gains on patient outcome in EwS and other undifferentiated sarcomas (10, 51). However, in our large EwS Cohort 1, *MYC* expression was not significantly associated with overall patient survival (*P*=0.689, **Supplementary Figure 1c**, **Supplementary Table 1**). Similarly, the chr8-located gene *RAD21*, previously reported to promote EwS tumorigenicity by mitigating EWSR1::FLI1-induced replication stress (23), did not show a significant association with overall EwS patient survival (*P*=0.174; **Supplementary Figure 1c**, **Supplementary Table 1**). These findings suggest that the mechanisms underlying the association of chr8 gain with EwS aggressiveness are more complex than previously anticipated.

To identify chr8-encoded genes most strongly associated with poor overall survival in EwS patients, we conducted a batch analysis within Cohort 1. Using our custom code software GenEx, we calculated *P*-values for the association between gene expression and overall survival for all microarray-represented genes, employing Mantel-Haenszel statistics (**Supplementary Table 1**).

Among all chromosome 8 located genes analyzed, EIF4EBP1 expression showed the strongest association with patient outcome, with high EIF4EBP1 expression significantly correlating with unfavorable overall survival (nominal P < 0.0001; Bonferroni-adjusted P = 0.049; Figure 1d,e; Supplementary Table 2). High EIF4EBP1 expression remained significantly associated with poor overall survival even when considering only patients with localized disease (P=0.0013, Figure 1e). Additionally, EIF4EBP1 ranked within the top 15 survival associated genes genome-wide (Figure 1d, Supplementary Table 1). These results are in consistence with the association of chr8 gain with poor overall survival in EwS patients (Figure 1b,c) as well as with previous research that has linked chr8p, where EIF4EBP1 is located, with EwS relapse (51, 52). Furthermore, EIF4EBP1 expression is significantly correlated with high ssGSEA enrichment scores for chr8 gene expression in Cohort 1 (P<0.001, Pearson's r = 0.47, Cohen's d = 1.19, **Supplementary Table 3**). This suggests that a significant part of the negative prognostic effect of the high chr8 gene expression signature can be attributed to high EIF4EBP1 expression. Accordingly, the predicted chr8 gain is significantly associated with elevated EIF4EBP1 expression levels in this cohort (P<0.001; Figure 1f), which also holds true when only considering patients that show an exclusive predicted chr8 gain or none of the above-mentioned other CNVs (P<0.001; Supplementary Figure 1d). This association was confirmed on mRNA and protein level in the independent Cohort 2 with chr8 status detected at the DNA level (P<0.001; Figure 1g, Supplementary Figure 1e). Similar to our analyses shown in Figure 1c, we reanalyzed our survival data from Cohort 1 now only focusing on exclusively predicted chr8 gained samples versus samples without any recurrent chromosomal gain/loss, which fully confirmed the prognostic role of EIF4EBP1 in EwS patients (Figure 1h). Interestingly, DEG analysis of Cohort 1 comparing chr8 high and low gene expression revealed that among genes of the mTOR signaling pathway, EIF4EBP1 is distinctively upregulated in tumors with chr8 gain (Supplementary Figure 1f), indicating that 4E-BP1 has a distinct clinical and functional role within the mTOR signaling pathway in EwS.

To evaluate the potential clinical and functional significance of chr8 gain and *EIF4EBP1* expression in other cancer entities besides EwS, we analyzed CNV data from DNA methylation arrays of The Cancer Genome Atlas (TCGA). Our analysis revealed that numerous cancer entities exhibit chr8 gains (specifically, 8 out of 32 identified entities exhibit chr8 gains in more than 10% of cases) (**Supplementary Table 4**). Additionally, in consistency with previously published data(46), chr8 gain and high *EIF4EBP1* expression are associated with unfavorable patient survival in several other cancer entities (chr8 gain in 4 and high *EIF4EBP1* expression in 14 out of 32 identified entities) (**Supplementary Table 4**). These include hepatocellular carcinoma, renal papillary cell carcinoma, lower-grade glioma, and thymoma (**Supplementary Table 4**).

Collectively, these results indicate that chr8 gain contributes to unfavorable outcomes of EwS patients and identify 4E-BP1 as a potential driver of EwS aggressiveness encoded on chr8.

#### 4E-BP1 drives a proliferation-associated proteomic network

Contrary to our findings that high *EIF4EBP1* levels significantly correlated with worse patient outcome (**Figure 1d,e,h**), a recent report has suggested that 4E-BP1 may act as a tumor suppressor in EwS (53). However, this conclusion was based on observations upon supraphysiological, ectopic overexpression of a phospho-mutant (and thus functionally hyperactive) 4E-BP1 protein in two EwS cell lines (EW8 and TC-71) (53). The role of 4E-BP1 in cancer is complex and strongly depends on the cellular context and its precise phosphorylation status(30). Therefore, to obtain a more comprehensive understanding of 4E-BP1 in EwS, we first integrated results of pre-ranked fast Gene Set Enrichment Analyses (fGSEA). We conducted fGSEAs based on Pearson's correlation coefficients between the mRNA expression levels of *EIF4EBP1* and every other gene represented in the respective datasets of Cohort 1 and 2 (**Supplementary Table 5,6**). Additionally, we carried out a third fGSEA based on gene expression fold-changes (FCs) between tumors with and without detected chr8 gain in Cohort 2 (**Supplementary Table 7**). The overlap between all three fGSEAs consisted predominantly of proliferation-associated gene sets (**Figures 2a,b, Supplementary Table** 

**5-7**). These transcriptomic data from EwS patients pointed toward a role of 4E-BP1 in the regulation of EwS cell proliferation and strongly supported the potential role of 4E-BP1 as a major mediator of chr8 gain-driven poor prognosis in EwS.

To further explore this hypothesis, we generated an in vitro 4E-BP1 knockdown model in three EwS cell lines with relatively high *EIF4EBP1* baseline expression levels (A-673, SK-N-MC, and TC-71) (Supplementary Figure 2a). Notably, two of the selected cell lines (SK-N-MC and TC-71) exhibit a chr8 gain (26). Since chr8 gains are most probably not the only factor impacting on 4E-BP1 expression levels, and certainly not all chr8 gained tumors necessarily show high 4E-BP1 expression levels, we intentionally included one cell line (A-673) without chr8 amplification in the following analyses to emphasize the functional and clinical relevance of 4E-BP1 by itself across EwS with and without chr8 gain. Furthermore, A-673 cells were employed because chr8 gain might as well affect expression levels of many other genes and thereby could bias the effects seen by modulation of 4E-BP1. To that end, we transduced these three EwS cell lines with a lentivirus containing a vectorsystem (pLKO Tet-on) with doxycycline (Dox)-inducible shRNAs, specifically directed against EIF4EBP1 (sh4E-BP1 1 or sh4E-BP1 2) or a non-targeting control shRNA (shCtr). Both targeted shRNAs effectively silenced EIF4EBP1 mRNA expression, resulting in a strong knockdown of EIF4EBP1 mRNA levels (Supplementary Figure 2b) and protein levels (Figure 2c, Supplementary Figure 2c). This is consistent with a strong correlation between (EIF)4E-BP1 mRNA and protein levels in human cells, as evidenced by the analysis of Cancer Dependency Map (DepMap) gene expression and corresponding protein array data (n=887 cancer cell lines,  $r_{Pearson}$ =0.68, P=5.2×10<sup>-22</sup>). Western blot experiments demonstrated that knockdown of 4E-BP1 led to a consistent loss of its phosphorylated form (Ser65) in all EwS cell lines in similar manner as total 4E-BP1 (Supplementary Figure 2d,e). Therefore, our EwS 4E-BP1 knockdown models are well suited to study the functional consequences of its inactivation.

As 4E-BP1 regulates mRNA translation initiation by binding to the translation initiation factor eIF4E and thereby modifying overall and selective translation rates (30), we asked whether functional interference with 4E-BP1 might also affect proliferation-related translational signatures. To identify proteins regulated by 4E-BP1 exclusively at the translational level, we combined mass spectrometry (MS) based proteomic profiling of newly synthesized proteins (pulsed SILAC) with parallel transcriptome profiling by gene expression microarrays. To this end, we silenced 4E-BP1 in three EwS cell lines (A-673, SK-N-MC, and TC-71) and pulsed them with stable isotope labeled amino acids in cell culture (SILAC) medium and the methionine analog L-Azidohomoalanine (AHA) for 6 h. We identified 9,508 proteins through MS analysis, of which 4,335 common proteins across all cell lines and constructs with at least one value per replicate group were used for downstream analyses. Our parallel microarray analyses captured 12,056 stably expressed genes across all three cell lines. Following further filtering steps (see methods section), we identified 1,332 differentially expressed proteins upon 4E-BP1 knockdown (adj. P-value < 0.05), which were not regulated by 4E-BP1 at the mRNA level across all three cell lines (Supplementary Table 8). To technically validate our MS findings, we conducted western blot analyses for one representative upregulated protein, PDCD4 (54-57), following 4E-BP1 knockdown, thereby providing independent confirmation of our results using an alternative method (Supplementary Figure 2f). Preranked fGSEA analysis on proteins not regulated at the mRNA level, and therewith most likely directly differentially regulated by 4E-BP1, identified again a strong enrichment of proliferationassociated gene sets (Figure 2d, Supplementary Table 9) consistent with fGSEA results from patient gene expression data as shown in Figure 2a,b. Such integrative fGSEA analyses conducted using the full list of obtained proteins and genes, respectively, are displayed in Supplementary **Tables 10,11** and essentially showed similar results.

Our *in silico* analyses of patient data at the mRNA level and functional *in vitro* analyses at the protein level collectively indicate that 4E-BP1 is linked to accelerated proliferation of EwS cells, suggesting a potential role as an oncogene in EwS.

#### 4E-BP1 promotes proliferation and tumorigenicity of EwS cells

To confirm the pro-proliferative and oncogenic role of 4E-BP1 in EwS, we conducted various functional in vitro and in vivo assays. We found that knockdown of 4E-BP1 for 96 h significantly inhibited cell proliferation in all three cell lines (Figure 3a). The anti-proliferative effect of 4E-BP1 knockdown appeared to be independent of cell death as Trypan-Blue-exclusion assays did not consistently show a significant effect of 4E-BP1 knockdown on cell death across all cell lines and shRNAs (Supplementary Figure 3a). Prolonged 4E-BP1 knockdown (10–14 d) significantly reduced both 2D clonogenic and 3D anchorage-independent growth of EwS cells (Figure 3b.c). Such effects were not observed in shCtr cells (Figure 3b,c). Similarly, knockdown of 4E-BP1 in subcutaneously xenotransplanted cells significantly reduced tumor growth in vivo (Figure 3d, Supplementary Figure 3b, Supplementary Table 12). Consistent with our in vitro results, this phenotype was linked to a significantly diminished mitotic cell count, as revealed by histologic assessment of the respective xenografts (Figure 3e, Supplementary Figure 3c). No difference in tumor necrosis was observed between xenografts with or without 4E-BP1 knockdown (Supplementary Figure 3d). Notably, combined MS and gene expression profiling of A-673 and TC-71 xenografts validated the pro-proliferative proteo-transcriptomic signatures by fGSEA as observed in vitro (Supplementary Tables 13,14). To validate the effect of 4E-BP1 in an orthotopic xenograft model, we xenografted TC-71 cells transduced with an inducible EIF4EBP1 targeting shRNA construct (sh4E-BP1 2) into the proximal tibia of NSG mice, which were subsequently treated with or without Dox. Similar to our subcutaneous xenograft model, the tumor burden in orthotopic EwS xenografts decreased upon Dox-induced knockdown of 4E-BP1 (Figure 3f). In summary and in conjunction with our integrative clinical and in silico analyses from patient tumors and cell line models (Figure 1 and 2), these results generated in vitro and in vivo provide strong evidence that 4E-BP1 acts as an oncogene in EwS.

#### High 4E-BP1 expression sensitizes for CDK4/6 inhibitor treatment

To identify therapeutic vulnerabilities in EwS with high 4E-BP1 expression, we conducted drug screens on 3D-spheroids of A-673 EwS cells with/without knockdown of 4E-BP1. Ribociclib, an FDA-approved CDK4/6 inhibitor(58–61), was the top hit demonstrating differential sensitivity in 4E-BP1 high expressing cells (Supplementary Figure 4a). The presented data align with the published gene-dependency data of DepMap project, indicating a significant and selective dependency of EwS cell lines on CDK4 expression compared to non-EwS cell lines (Supplementary Figure 4b). We validated these findings in 2D culture experiments using A-673 EwS cells with or without 4E-BP1 knockdown, and confirmed them in both A-673 and TC-71 EwS cells treated with the second FDA-approved CDK4/6 inhibitor, Palbociclib (Figure 4a, Supplementary Figure 4c) (58–61). The top three hits identified in the drug screen following Ribociclib (Vincristine, Thioguanine, and Methotrexate) exhibited no or comparatively lower increases in sensitivity upon 4E-BP1 knockdown in 2D experiments (Supplementary Figure 4d). Interestingly, EwS cell lines with high endogenous 4E-BP1 expression (A-673 and TC-71) showed greater sensitivity to Palbociclib and Ribociclib than cell lines with low endogenous 4E-BP1 expression (EW-22 and CHLA-10) (Figure 4b, Supplementary Figure 4e). Consistently, overexpression of 4E-BP1 in a EwS cell line expressing 4E-BP1 at a low endogenous level (EW-22) led to an increase of sensitivity toward CDK4/6 inhibition (Supplementary Figure 4f). Next, we conducted xenograft experiments by transplanting A673 EwS cells subcutaneously into the flanks of NSG mice, treated with/without Dox and with/without Palbociclib, whereby treatment started when tumors were palpable in all mice. Xenografts with 4E-BP1 knockdown and xenografts with Palbociclib treatment similarly exhibited a very strong reduction of tumor growth, which correlated with a strong decrease in histologically assessable viable tumor burden as compared to respective xenografts without 4E-BP1 knockdown or Palbociclib treatment (Figures 4c,d, Supplementary Figure 4g, Supplementary Tables 15,16). Consistently, xenografts of mice with 4E-BP1 knockdown or treatment with Palbociclib, for which histological material was obtainable,

showed a lower number of mitoses per high-power field (Figure 4e). However, since the very strong growth-inhibitory effects of either 4E-BP1 knockdown or Palbociclib treatment alone precluded the assessment of a potential differential effect of 4E-BP1 expression on sensitivity toward Palbociclib in this model (Figures 4c,d, Supplementary Figure 4g, Supplementary Tables 15,16), we turned for further validation to patient-derived real-world data. To this end, we analyzed gene expression and 3D drug sensitivity data from 14 EwS patient-derived short-term cultures treated with Palbociclib or Ribociclib in the context of the Individualized Therapy For Relapsed Malignancies in Childhood (INFORM) registry(62). Strikingly, we found that high EIF4EBP1 expression is indeed associated with higher sensitivity toward CDK4/6 inhibitor treatment (Figure 4f). To more mechanistically decipher the link between high 4E-BP1 expression, EwS cell proliferation, and increased sensitivity toward CDK4/6 inhibitors, we screened the top 10% of downregulated proteins upon 4E-BP1 knockdown in our generated MS profiling (n=393) according to a reported potential direct or indirect regulatory association with CDK4/6 signaling (n=35). Furthermore, we screened for significant association of the transcript expression of these genes with poor overall survival in Cohort 1 (n=11). Among the remaining 11 proteins, we further focused on those with potential mechanistic association with CDK4/6 by literature, leading to a final selection of 6 proteins: CDC25B (63), PRMT5 (64, 65), MCM2 (66, 67), RBL1 (68, 69), RNF2 (70, 71), and USP14 (72–74). To validate these results we performed an association analysis with STRING(75), showing a close association of most of these genes with 4E-BP1 and CDK4/6 (Supplementary Figure 4h). Furthermore, we performed complementary western blot and parallel qRT-PCR assays measuring PRMT5 expression levels upon 4E-BP1 knockdown, showing that PRMT5 expression is reduced at the protein level, but not at the mRNA level. These results validate our integrated pulsed SILAC and transcriptomic analyses, reinforcing the conclusion that the observed changes in protein abundance are primarily regulated at the level of protein synthesis (Supplementary Figure 4i). We performed siRNA-mediated knockdown experiments for these genes in A-673 EwS cells, showing that knockdown of CDC25B, PRMT5, and RBL1 significantly reduced cell proliferation,

without affecting cell death (**Supplementary Figure 4i-k**), while there was no significant effect on proliferation or cell death upon knockdown of the remaining 3 genes (data not shown). To validate these genes as critical mediators of 4E-BP1-related increased CDK4/6 inhibitor sensitivity, we performed 2D drug sensitivity assays, showing that knockdown of CDC25B and PRMT5 is associated with a reduction of sensitivity toward CDK4/6 inhibition (**Supplementary Figure 4I**). In summary, these results suggest that 4E-BP1 may serve as a valuable predictive biomarker for clinical effectiveness of CDK4/6 inhibitor treatment.

#### **DISCUSSION**

The data presented herein in the EwS model establish chr8 gain as an unfavorable prognostic factor, primarily mediated through the overexpression of the translation initiation factor binding protein 4E-BP1, which guides pro-proliferative proteomic signatures and sensitizes cells to targeted CDK4/6 inhibitor treatment.

In precision oncology, it is crucial to decipher mechanisms underlying inter-tumoral heterogeneity to refine diagnostic and therapeutic algorithms (14, 76, 77). In this context, the identification of chr8 gain as a prognostic factor emphasizes the relevance of cytogenetic testing, which may help stratify patients into prognostic and/or therapeutic subgroups. Although chr8 trisomies are observed in approximately 50% of EwS patients, so far, only trends or moderate associations between whole chr8 gain (i.e., trisomies) and poor patient outcome have been observed (21, 23–25, 51, 78, 79). Our data provide a significant association between a high chr8 gene expression signature and poor overall survival of EwS patients, whereby strikingly, this association was even more pronounced when only exclusively considering patients without potentially confounding additional chromosomal gains and losses (**Figure 1**). Importantly, this association also remains statistically significant even when only considering patients with localized disease (**Figure 1**). Therefore, chr8 gain, as assessed by cytogenetic testing or fluorescence in situ hybridization (FISH) or a high chr8 gene expression signature score (i.e., as assessed by ssGSEA), might serve as a prognostic biomarker

for poor overall patient survival. Consequently, it could be particularly useful for stratifying patients with localized disease into different treatment groups. Our results are consistent with studies from other cancer entities that have shown a prognostic/predictive value of chr8 gain, as for example in acute myeloid leukemia (6) and chronic myeloid leukemia (4, 5). Interestingly, chr8 gain is also observed in several specific other sarcoma entities, including myxoid liposarcoma (9), clear cell sarcoma (8), and pediatric undifferentiated sarcomas (10), as well as in several other cancer entities as shown in our analyses of TCGA data with partial prognostic value (Supplementary Table 4). Partial gains or losses of chromosome 8 have been described in a broad range of cancer entities, such as prostate, lung, hepatocellular, and renal cell carcinoma (80–84). In contrast to the reported data from EwS, in some other cancer entities, chr8p losses are described to be associated with unfavorable clinical parameters (82, 84, 85). In the case of chr8q, gains are most frequently described as having tumor promoting functions due to resulting MYC amplification (80, 83, 84, 86). However, in our patient cohort, a clinical association between MYC expression and overall survival was not evident (Supplementary Figure 1c, Supplementary Table 1), although MYC expression was linked to the expression of the proliferation marker Ki-67 and clinical outcome in EwS (87). Similarly, we could not show a significant association with overall patients survival for the chr8located gene RAD21 in our patient cohort (Supplementary Figure 1c, Supplementary Table 1), which was previously reported to promote EwS tumorigenicity by mitigating EWSR1::FLII-induced replication stress (23). However, although we could not show a significant association of the expression of those genes with overall survival, it is conceivable that the biological effect of these genes is not necessarily linked to their mRNA abundance and is more determined by their absolute expression levels.

Our results show that poor survival outcomes associated with chr8 gains are primarily mediated by 4E-BP1 orchestrating a pro-proliferative proteomic network. However, the role of 4E-BP1 in cancer initiation/progression, especially whether 4E-BP1 exerts a pro-tumorigenic or tumor suppressing function, is still discussed controversially, appears to be context-dependent, and is not yet definite

(30). 4E-BP1 has mostly been regarded as exerting tumor suppressing functions by blocking capdependent translation or selective inhibition of specific transcript translation, and consistently, high levels of phosphorylated (and thus inactive) 4E-BP1 has been associated with poor outcome in many cancer entities (30, 43, 44). However, 4E-BP1 cannot be regarded as a bona fide tumor suppressor since 4E-BP1 knockout mice failed to develop tumors (88) and increasing evidence suggests that the role of 4E-BP1 in cancer is more complex. In a context-dependent manner, 4E-BP1 can as well exert pro-tumorigenic functions, such as promotion of hypoxia-induced angiogenesis and tumor formation in breast cancer (37) or conferring protection toward glucose starvation in glioma (42), both by selectively regulating translation of specific transcripts. Furthermore, it has been shown that 4E-BP1 is required for RAS-induced transformation in a p53-dependent manner (45). The data presented here in EwS are in favor of a tumor promoting role of 4E-BP1, regulating a proproliferative proteomic network in EwS (Figure 2,3). This is consistent to our results showing a strong association of high EIF4EBP1 expression levels with poor EwS survival (Figure 1). Such association is as well evident in numerous other cancer entities as shown in our analysis of TCGA data (Supplementary Table 4) and is consistent to prior published deep computational analysis on pan-cancer TCGA data (46). However, the observed variances in 4E-BP1 mRNA and protein expression levels in patient tumors stratified by chr8 status (Figure 1f,g) suggest that chr8 gains may not be the only factor impacting on 4E-BP1 expression levels in EwS. Apart from chr8 gains, other possible mechanisms of EIF4EBP1 upregulation, such as direct upregulation driven by differential transcription factor binding, have been described across cancer entities and may as well account for high 4E-BP1 expression levels in individual tumors (14, 89).

We demonstrate that high 4E-BP1 expression levels sensitize EwS cells to CDK4/6 inhibitor treatment with Palbociclib and Ribociclib (**Figure 4**). This effect may be mediated through direct translational regulation of CDC25B, a protein phosphatase critical for cell cycle progression and reported to contribute to tumorigenesis across multiple cancer types (63), and PRMT5, a methyltransferase that regulates diverse cellular processes, particularly transcription, and is similarly

implicated in the progression of various malignancies (64, 65). Especially PRMT5 is described to play an important role in mediation of CDK4/6 inhibitor sensitivity (64). Palbociclib and Ribociclib are FDA-approved for the treatment of hormone receptor positive, human epidermal growth factor receptor 2 (EGFR2, alias HER2) negative advanced or metastatic breast cancer, used in combination with an aromatase inhibitor in postmenopausal women (58–61). In addition to their prognostic value in EwS (Figure 1), chr8 gain and, specifically, 4E-BP1 expression might serve as predictive markers to subject EwS patients into a CDK4/6-inibitor sensitive and non-sensitive group. Such tailored stratification of patients into specific targeted treatment groups with already FDA-approved drugs could significantly and promptly improve EwS patient outcome within the context of precision oncology. Notably, preclinical studies have already described a general sensitivity of EwS toward CDK4/6 inhibition, whereby IGF-1R activation can mediated CDK4/6 inhibitor resistance (90, 91). As a result, a phase II clinical trial recently investigated Palbociclib in combination with the IGF-1R inhibitor Ganitumab for patients with relapsed or refractory EwS, reporting a lack of adequate therapeutic activity although a subgroup of patients showed prolonged stable disease (92). However, this study did not include patient stratification based on predictive biomarkers. This gap might be addressed in future studies by incorporating predictive testing for chr8 gain and especially 4E-BP1 expression. Also, potential synergistic combination therapies might be needed to achieve full clinical effectiveness of CDK4/6 inhibition, which warrant further preclinical and clinical evaluation. The clinical importance of our findings is further pronounced by the currently ongoing Pfizer phase II trial testing treatment with Irinotecan and Temozolomide with/without Palbociclib in EwS patients (https://clinicaltrials.gov/study/NCT03709680) (93). However, the fact that high 4E-BP1 expression can be also observed in some tumor samples and cell lines without chr8 gains may hint to other factors may also contribute to its high expression and suggest that high 4E-BP1 expression may serve as a more robust predictive biomarker for response to CDK4/6 inhibitors than chr8 gains per se. While our data suggest that 4E-BP1 expression may, to some extent, enhance sensitivity to conventional chemotherapeutic agents, our primary focus is on the identification of targeted

therapies whose efficacy is dependent on 4E-BP1 expression levels. This approach aims to inform the development of novel therapeutic strategies that could either reduce the adverse effects associated with standard chemotherapy or act synergistically with established treatment regimens in Ewing sarcoma therapy. Yet, it should be noted that chr8 gains may have broad functional effects that go beyond those of 4E-BP1 and its association with CDK4/6-sensitivity. Thus, CDK4/6 inhibition may only address part of the chr8 gain-mediated effects. Future studies will need to dissect the other chr8-dependent phenotypes and how they crosslink with those mediated by 4E-BP1. Collectively, our data suggest that chr8 gain plays an important prognostic role in EwS and that its functional effects on tumor progression are primarily driven by increased 4E-BP1 expression mediating a pro-proliferative phenotype. Since chr8 gain occurs in approximately 50% of EwS cases, our results indicate that this chromosomal aberration is a major source of inter-tumoral heterogeneity shaping the disease phenotype, clinical outcomes, and therapy options in EwS. Consequently, further cytogenetic testing of EwS might offer a refinement of clinical management within the context of precision oncology.

#### MATERIALS AND METHODS

Please see Supplementary Information for Materials and Methods.

#### Sex as a biological variable

Male and female mice were used for *in vivo* experiments. Male and female patients were included in patient data analyses.

#### Study approval

Animal experiments were approved by the government of Upper Bavaria and North Baden and conducted in accordance with ARRIVE guidelines, recommendations of the European Community

(86/609/EEC), and United Kingdom Coordinating Committee on Cancer Research (UKCCCR) guidelines for the welfare and use of animals in cancer research.

#### **Data availability**

Microarray data is publicly available under accession numbers GSE294433 and GSE295817 at the Gene Expression Omnibus (GEO). MS datasets were uploaded at the PRIDE portal and are publicly accessible under the project accession code PXD065282. A 'Supporting data values' file was provided in the Supplementary Data.

#### **CONCLUSIONS**

Collectively, we establish chr8 gains and high 4E-BP1 expression as prognostic biomarkers in EwS and demonstrate that their association with patient outcome is primarily mediated by 4E-BP1 orchestrating a pro-proliferative proteomic network sensitizing EwS for CDK4/6-inhibitors. Since chr8 gains occur in approximately 50% of EwS cases, our results indicate that this chromosomal aberration is a major source of inter-tumoral heterogeneity shaping the disease phenotype, clinical outcomes, and therapy options in EwS. Consequently, our data suggest that testing for chr8 gains may improve risk-stratification and therapeutic management in EwS and other cancers in the context of precision oncology.

#### **AUTHOR CONTRIBUTIONS**

C.M.F. and A.C.E. performed functional *in vitro* and *in vivo* experiments, as well as bioinformatic and histological analyses, analyzed and interpreted all data, designed all Figures, and wrote the paper. M.F.O. performed functional experiments, helped in shRNA design and lentiviral transduction of cell lines. K.A. performed MS and analyzed MS data. J.S. and A.Y. helped in dataset curation. J.L. helped in conduction of *in vivo* experiments. T.L.B.H., F.H.G., M.M.L.K., E.V., A.K.C. assisted in experimental procedures. R.W. performed cloning of vectors. F.W. performed

analyses of histology. F.Z. assisted in experimental procedures. S.O., R.I., A.B. helped in performance of in vivo experiments. J.A., A.S., W.H., U.D. provided clinical information. M.S. provided financial support and laboratory infrastructure. O.W., I.O., H.P., and A.L. performed drug screens. S.M.P., G.L. provided biological and technical guidance. L.R.-P. conducted methylation arrays and performed bioinformatic analyses. J.K. provided financial support and laboratory infrastructure for performance of MS. F.-C.A. carried out functional in vitro and in vivo experiments. J.M. coordinated and supervised the study, provided biological and technical guidance, performed functional experiments as well as bioinformatic and histological analyses, analyzed and interpreted all data, wrote the paper, and provided financial support. T.G.P.G designed, coordinated, and supervised the study, provided biological and technical guidance, analyzed and interpreted all data, wrote the paper and provided financial support and laboratory infrastructure. All authors read and approved the final manuscript. The contributions of the first two authors to this work were highly comparable in significance. Given the similarity in the amount and importance of their contributions, it was not possible to differentiate qualitatively between them. Therefore, we have designated shared-first authorship. C.M.F. is listed in first position and A.C.E. in second position to reflect a modest difference in the overall quantity of work performed.

#### **ACKNOWLEDGEMENTS**

We thank Dr. Aruna Marchetto for her help in western blot assays. We thank Dr. Clemens M. Lechner for statistical advice. Support by the DKFZ Light Microscopy Facility is gratefully acknowledged. We thank Luuk A. Broeils and Dr. Sebastiaan van Heesch for additional proteomic advice.

#### **DECLARATIONS**

#### **Competing interests**

The authors have declared that no conflict of interest exists.

#### **Funding**

This project was mainly supported by a grant from the German Cancer Aid (DKH-70112257 to T.G.P.G.). The laboratory of T.G.P.G. is further supported by grants from the Matthias-Lackas foundation, the Dr. Leopold und Carmen Ellinger foundation, the Gert & Susanna Mayer foundation, the Deutsche Forschungsgemeinschaft (DFG 458891500), the German Cancer Aid (DKH-7011411, DKH-70114278, DKH-70115315), the Dr. Rolf M. Schwiete foundation, the SMARCB1 association, the Ministry of Education and Research (BMBF; SMART-CARE, and HEROES-AYA), and the Barbara and Wilfried Mohr foundation. The laboratory of T.G.P.G. is co-funded by the European Union (ERC, CANCER-HARAKIRI, 101122595), views and opinions expressed are however those of the authors only and do not necessarily reflect those of the European Union or the European Research Council, neither the European Union nor the granting authority can be held responsible for them. J.M., I.O., O.W., M.S., A.B., and U.D. (01KD2207B) were supported by the Ministry of Education and Research (HEROES-AYA). J.M. was additionally supported by the Heidelberg Foundation of Surgery and the Barbara und Wilfried Mohr foundation. J.L. was supported by a scholarship of the China Scholarship Council (CSC) and C.M.F. and A.C.E. by scholarships of the German Cancer Aid and the German Academic Scholarship Foundation. T.L.B.H. acknowledges a scholarship of the German Cancer Aid, and E.V. a scholarship of the Heinrich F.C. Behr foundation. Furthermore, this work was supported by grants of the German Cancer Aid (DKH-108128 and DKH-70113419) to U.D. The laboratory of J.A. was supported by grants from the Instituto de Salud Carlos III (PI20CIII/00020; DTS22CIII/00003; PMP21-00073), Fundación La Marató de TV3 (201937-30-31), Asociación Pablo Ugarte, Fundación Sonrisa de Alex, Asociación Todos somos Iván, and Asociación Candela Riera.

#### **REFERENCES**

- 1. Ben-David U, Amon A. Context is everything: aneuploidy in cancer. *Nat Rev Genet*. 2020;21(1):44–62.
- 2. Gordon DJ, Resio B, Pellman D. Causes and consequences of aneuploidy in cancer. *Nat Rev Genet*. 2012;13(3):189–203.
- 3. Vasudevan A, et al. Aneuploidy as a promoter and suppressor of malignant growth. *Nat Rev Cancer*. 2021;21(2):89–103.
- 4. Wang W, et al. Impact of trisomy 8 on treatment response and survival of patients with chronic myelogenous leukemia in the era of tyrosine kinase inhibitors. *Leukemia*. 2015;29(11):2263–2266.
- 5. Wang W, et al. Clinical significance of trisomy 8 that emerges during therapy in chronic myeloid leukemia. *Blood Cancer J.* 2016;6(11):e490.
- 6. Wolman SR, et al. Impact of trisomy 8 (+8) on clinical presentation, treatment response, and survival in acute myeloid leukemia: a Southwest Oncology Group study. *Blood*. 2002;100(1):29–35.
- 7. Panani AD, et al. Numerical aberrations of chromosome 8 in gastric cancer detected by fluorescence in situ hybridization. *Anticancer Res.* 2004;24(1):155–159.
- 8. Mrózek K, et al. Translocation t(12;22)(q13;q12.2-12.3) in a clear cell sarcoma of tendons and aponeuroses. *Genes Chromosomes Cancer*. 1993;6(4):249–252.
- 9. Sreekantaiah C, et al. Trisomy 8 as a nonrandom secondary change in myxoid liposarcoma. *Cancer Genet Cytogenet*. 1991;51(2):195–205.
- 10. Selvarajah S, et al. Characterization of trisomy 8 in pediatric undifferentiated sarcomas using advanced molecular cytogenetic techniques. *Cancer Genet Cytogenet*. 2007;174(1):35–41.
- 11. Dehner C, et al. Chromosome 8 gain is associated with high-grade transformation in MPNST. *JCI Insight*. 2021;6(6):e146351, 146351.
- 12. Grünewald TGP, et al. Ewing sarcoma. Nat Rev Dis Primer. 2018;4(1):5.
- 13. Grünewald TGP, et al. Chimeric EWSR1-FLI1 regulates the Ewing sarcoma susceptibility gene EGR2 via a GGAA microsatellite. *Nat Genet*. 2015;47(9):1073–1078.
- 14. Musa J, et al. Cooperation of cancer drivers with regulatory germline variants shapes clinical outcomes. *Nat Commun*. 2019;10(1):4128.
- 15. Machiela MJ, et al. Genome-wide association study identifies multiple new loci associated with Ewing sarcoma susceptibility. *Nat Commun*. 2018;9(1):3184.
- 16. Tirode F, et al. Genomic landscape of Ewing sarcoma defines an aggressive subtype with coassociation of STAG2 and TP53 mutations. *Cancer Discov.* 2014;4(11):1342–1353.
- 17. Brohl AS, et al. The genomic landscape of the Ewing Sarcoma family of tumors reveals recurrent STAG2 mutation. *PLoS Genet*. 2014;10(7):e1004475.

- 18. Crompton BD, et al. The genomic landscape of pediatric Ewing sarcoma. *Cancer Discov*. 2014;4(11):1326–1341.
- 19. Mugneret F, et al. Chromosomes in Ewing's sarcoma. II. Nonrandom additional changes, trisomy 8 and der(16)t(1;16). *Cancer Genet Cytogenet*. 1988;32(2):239–245.
- 20. Maurici D, et al. Frequency and implications of chromosome 8 and 12 gains in Ewing sarcoma. *Cancer Genet Cytogenet*. 1998;100(2):106–110.
- 21. Armengol G, et al. Recurrent gains of 1q, 8 and 12 in the Ewing family of tumours by comparative genomic hybridization. *Br J Cancer*. 1997;75(10):1403–1409.
- 22. Nacev BA, et al. Clinical sequencing of soft tissue and bone sarcomas delineates diverse genomic landscapes and potential therapeutic targets. *Nat Commun*. 2022;13(1):3405.
- 23. Su XA, et al. RAD21 is a driver of chromosome 8 gain in Ewing sarcoma to mitigate replication stress. *Genes Dev.* 2021;35(7–8):556–572.
- 24. Tarkkanen M, et al. Clinical correlations of genetic changes by comparative genomic hybridization in Ewing sarcoma and related tumors. *Cancer Genet Cytogenet*. 1999;114(1):35–41.
- 25. Hattinger CM, et al. Prognostic impact of chromosomal aberrations in Ewing tumours. *Br J Cancer*. 2002;86(11):1763–1769.
- 26. Orth MF, et al. Systematic multi-omics cell line profiling uncovers principles of Ewing sarcoma fusion oncogene-mediated gene regulation. *Cell Rep.* 2022;41(10):111761.
- 27. Mackintosh C, et al. 1q gain and CDT2 overexpression underlie an aggressive and highly proliferative form of Ewing sarcoma. *Oncogene*. 2012;31(10):1287–1298.
- 28. Kullendorff CM, et al. Cytogenetic aberrations in Ewing sarcoma: are secondary changes associated with clinical outcome? *Med Pediatr Oncol.* 1999;32(2):79–83.
- 29. Goodspeed A, et al. Single cell RNA-sequencing of Ewing sarcoma tumors demonstrates transcriptional heterogeneity and clonal evolution [preprint]. 2024;2024.01.18.576251.
- 30. Musa J, et al. Eukaryotic initiation factor 4E-binding protein 1 (4E-BP1): a master regulator of mRNA translation involved in tumorigenesis. *Oncogene*. [published online ahead of print: February 1, 2016]. https://doi.org/10.1038/onc.2015.515.
- 31. Saxton RA, Sabatini DM. mTOR Signaling in Growth, Metabolism, and Disease. *Cell*. 2017;168(6):960–976.
- 32. Brito Querido J, et al. Structure of a human 48S translational initiation complex. *Science*. 2020;369(6508):1220–1227.
- 33. Truitt ML, et al. Differential Requirements for eIF4E Dose in Normal Development and Cancer. *Cell*. 2015;162(1):59–71.
- 34. Silvera D, Formenti SC, Schneider RJ. Translational control in cancer. *Nat Rev Cancer*. 2010;10(4):254–266.
- 35. Morita M, et al. mTORC1 controls mitochondrial activity and biogenesis through 4E-BP-dependent translational regulation. *Cell Metab.* 2013;18(5):698–711.

- 36. De Benedetti A, Graff JR. eIF-4E expression and its role in malignancies and metastases. *Oncogene*. 2004;23(18):3189–3199.
- 37. Braunstein S, et al. A hypoxia-controlled cap-dependent to cap-independent translation switch in breast cancer. *Mol Cell*. 2007;28(3):501–512.
- 38. Zid BM, et al. 4E-BP extends lifespan upon dietary restriction by enhancing mitochondrial activity in Drosophila. *Cell*. 2009;139(1):149–160.
- 39. Dowling RJO, et al. mTORC1-mediated cell proliferation, but not cell growth, controlled by the 4E-BPs. *Science*. 2010;328(5982):1172–1176.
- 40. Thoreen CC, et al. A unifying model for mTORC1-mediated regulation of mRNA translation. *Nature*. 2012;485(7396):109–113.
- 41. Hsieh AC, et al. The translational landscape of mTOR signalling steers cancer initiation and metastasis. *Nature*. 2012;485(7396):55–61.
- 42. Levy T, et al. mTORC1 regulates cell survival under glucose starvation through 4EBP1/2-mediated translational reprogramming of fatty acid metabolism. *Nat Commun*. 2024;15(1):4083.
- 43. Wang Z, et al. 4E-BP1 is a tumor suppressor protein reactivated by mTOR inhibition in head and neck cancer. *Cancer Res.* 2019;79(7):1438–1450.
- 44. Ding M, et al. The mTOR Targets 4E-BP1/2 Restrain Tumor Growth and Promote Hypoxia Tolerance in PTEN-driven Prostate Cancer. *Mol Cancer Res MCR*. 2018;16(4):682–695.
- 45. Petroulakis E, et al. p53-dependent translational control of senescence and transformation via 4E-BPs. *Cancer Cell*. 2009;16(5):439–446.
- 46. Wu S, Wagner G. Deep computational analysis details dysregulation of eukaryotic translation initiation complex eIF4F in human cancers. *Cell Syst.* 2021;12(9):907-923.e6.
- 47. Zhou X, et al. Classification of Muscle-Invasive Bladder Cancer Based on Immunogenomic Profiling. *Front Oncol.* 2020;10:1429.
- 48. Barbie DA, et al. Systematic RNA interference reveals that oncogenic KRAS-driven cancers require TBK1. *Nature*. 2009;462(7269):108–112.
- 49. Ferrari F, et al. PREDA: an R-package to identify regional variations in genomic data. *Bioinforma Oxf Engl.* 2011;27(17):2446–2447.
- 50. Li M, et al. TRAIP modulates the IGFBP3/AKT pathway to enhance the invasion and proliferation of osteosarcoma by promoting KANK1 degradation. *Cell Death Dis.* 2021;12(8):1–13.
- 51. Jahromi MS, Jones KB, Schiffman JD. Copy Number Alterations and Methylation in Ewing's Sarcoma. *Sarcoma*. 2011;2011:362173.
- 52. Ozaki T, et al. Genetic imbalances revealed by comparative genomic hybridization in Ewing tumors. *Genes Chromosomes Cancer*. 2001;32(2):164–171.
- 53. Goss KL, et al. The translational repressor 4E-BP1 regulates RRM2 levels and functions as a tumor suppressor in Ewing sarcoma tumors. *Oncogene*. 2021;40(3):564–577.

- 54. Dorrello NV, et al. S6K1- and betaTRCP-mediated degradation of PDCD4 promotes protein translation and cell growth. *Science*. 2006;314(5798):467–471.
- 55. Haas A, et al. PDCD4 controls the G1/S-phase transition in a telomerase-immortalized epithelial cell line and affects the expression level and translation of multiple mRNAs. *Sci Rep.* 2020;10(1):2758.
- 56. Wang Q, Yang H-S. The role of Pdcd4 in tumor suppression and protein translation. *Biol Cell*. 2018;10.1111/boc.201800014.
- 57. Jansen AP, Camalier CE, Colburn NH. Epidermal expression of the translation inhibitor programmed cell death 4 suppresses tumorigenesis. *Cancer Res.* 2005;65(14):6034–6041.
- 58. Morrison C. Pfizer's CDK4/6 inhibitor approved for advanced breast cancer [Internet]. *Nat Biotechnol.* 2015. https://doi.org/10.1038/nbt0415-323.
- 59. Asghar U, et al. The history and future of targeting cyclin-dependent kinases in cancer therapy. *Nat Rev Drug Discov*. 2015;14(2):130–146.
- 60. Sherr CJ, Beach D, Shapiro GI. Targeting CDK4 and CDK6: From Discovery to Therapy. *Cancer Discov.* 2016;6(4):353–367.
- 61. Mullard A. FDA approves Novartis's CDK4/6 inhibitor. Nat Rev Drug Discov. 2017;16(4):229-229.
- 62. van Tilburg CM, et al. The Pediatric Precision Oncology INFORM Registry: Clinical Outcome and Benefit for Patients with Very High-Evidence Targets. *Cancer Discov.* 2021;11(11):2764–2779.
- 63. Sur S, Agrawal DK. Phosphatases and kinases regulating CDC25 activity in the cell cycle: clinical implications of CDC25 overexpression and potential treatment strategies. *Mol Cell Biochem*. 2016;416(1–2):33–46.
- 64. AbuHammad S, et al. Regulation of PRMT5-MDM4 axis is critical in the response to CDK4/6 inhibitors in melanoma. *Proc Natl Acad Sci U S A*. 2019;116(36):17990–18000.
- 65. Lin C-C, et al. PRMT5 is an actionable therapeutic target in CDK4/6 inhibitor-resistant ER+/RB-deficient breast cancer. *Nat Commun*. 2024;15(1):2287.
- 66. Fan H, et al. DNA damage induced by CDK4 and CDK6 blockade triggers anti-tumor immune responses through cGAS-STING pathway. *Commun Biol.* 2023;6(1):1041.
- 67. Crozier L, et al. CDK4/6 inhibitors induce replication stress to cause long-term cell cycle withdrawal. *EMBO J.* 2022;41(6):e108599.
- 68. Beijersbergen RL, et al. Regulation of the retinoblastoma protein-related p107 by G1 cyclin complexes. *Genes Dev.* 1995;9(11):1340–1353.
- 69. Leng X, et al. Reversal of growth suppression by p107 via direct phosphorylation by cyclin D1/cyclin-dependent kinase 4. *Mol Cell Biol*. 2002;22(7):2242–2254.
- 70. Choi D, et al. Prohibitin interacts with RNF2 and regulates E2F1 function via dual pathways. *Oncogene*. 2008;27(12):1716–1725.
- 71. Pan L, et al. RNF2 mediates pulmonary fibroblasts activation and proliferation by regulating mTOR and p16-CDK4-Rb1 signaling pathway. *Inflamm Res Off J Eur Histamine Res Soc Al.* 2022;71(10–11):1283–1303.

- 72. Liao Y, et al. Proteasome-associated deubiquitinase ubiquitin-specific protease 14 regulates prostate cancer proliferation by deubiquitinating and stabilizing androgen receptor. *Cell Death Dis.* 2017;8(2):e2585.
- 73. Lee B-H, et al. USP14 deubiquitinates proteasome-bound substrates that are ubiquitinated at multiple sites. *Nature*. 2016;532(7599):398–401.
- 74. Hang C, et al. Ubiquitin-specific protease 14 (USP14) promotes proliferation and metastasis in pancreatic ductal adenocarcinoma. *J Mol Histol.* 2021;52(2):187–196.
- 75. Szklarczyk D, et al. The STRING database in 2023: protein-protein association networks and functional enrichment analyses for any sequenced genome of interest. *Nucleic Acids Res.* 2023;51(D1):D638–D646.
- 76. Garraway LA, Verweij J, Ballman KV. Precision oncology: an overview. *J Clin Oncol Off J Am Soc Clin Oncol*. 2013;31(15):1803–1805.
- 77. Musa J, Grünewald TGP. Interaction between somatic mutations and germline variants contributes to clinical heterogeneity in cancer. *Mol Cell Oncol*. 2020;7(1):1682924.
- 78. Brisset S, et al. CGH analysis of secondary genetic changes in Ewing tumors: correlation with metastatic disease in a series of 43 cases. *Cancer Genet Cytogenet*. 2001;130(1):57–61.
- 79. Ferreira BI, et al. Array CGH and gene-expression profiling reveals distinct genomic instability patterns associated with DNA repair and cell-cycle checkpoint pathways in Ewing's sarcoma. *Oncogene*. 2008;27(14):2084–2090.
- 80. Steiner T, et al. Gain in Chromosome 8q Correlates with Early Progression in Hormonal Treated Prostate Cancer. *Eur Urol.* 2002;41(2):167–171.
- 81. Baykara O, et al. Amplification of Chromosome 8 Genes in Lung Cancer. *J Cancer*. 2015;6(3):270–275.
- 82. Qin L-X, et al. The Association of Chromosome 8p Deletion and Tumor Metastasis in Human Hepatocellular Carcinoma1. *Cancer Res.* 1999;59(22):5662–5665.
- 83. Mehrazin R, et al. The correlation between gain of chromosome 8q and survival in patients with clear and papillary renal cell carcinoma. *Ther Adv Urol*. 2018;10(1):3–10.
- 84. El Gammal AT, et al. Chromosome 8p deletions and 8q gains are associated with tumor progression and poor prognosis in prostate cancer. *Clin Cancer Res Off J Am Assoc Cancer Res*. 2010;16(1):56–64.
- 85. Cai Y, et al. Loss of Chromosome 8p Governs Tumor Progression and Drug Response by Altering Lipid Metabolism. *Cancer Cell.* 2016;29(5):751–766.
- 86. Klatte T, et al. Gain of chromosome 8q is associated with metastases and poor survival of patients with clear cell renal cell carcinoma. *Cancer*. 2012;118(23):5777–5782.
- 87. Sollazzo MR, et al. Increased c-myc oncogene expression in Ewing's sarcoma: correlation with Ki67 proliferation index. *Tumori*. 1999;85(3):167–173.
- 88. Tsukiyama-Kohara K, et al. Adipose tissue reduction in mice lacking the translational inhibitor 4E-BP1. *Nat Med.* 2001;7(10):1128–1132.

- 89. Hauffe L, et al. Eukaryotic translation initiation factor 4E binding protein 1 (EIF4EBP1) expression in glioblastoma is driven by ETS1- and MYBL2-dependent transcriptional activation. *Cell Death Discov*. 2022;8(1):91.
- 90. Guenther LM, et al. A Combination CDK4/6 and IGF1R Inhibitor Strategy for Ewing Sarcoma. *Clin Cancer Res Off J Am Assoc Cancer Res.* [published online ahead of print: November 5, 2018]. https://doi.org/10.1158/1078-0432.CCR-18-0372.
- 91. Kennedy AL, et al. Functional, chemical genomic, and super-enhancer screening identify sensitivity to cyclin D1/CDK4 pathway inhibition in Ewing sarcoma. *Oncotarget*. 2015;6(30):30178–30193.
- 92. Shulman DS, et al. Phase 2 trial of palbociclib and ganitumab in patients with relapsed Ewing sarcoma. *Cancer Med.* 2023;12(14):15207–15216.
- 93. Laetsch TW, et al. Phase 2 study to evaluate palbociclib in combination with irinotecan and temozolomide in pediatric patients with recurrent or refractory Ewing sarcoma. *J Clin Oncol*. 2022;40(16\_suppl):TPS11583-TPS11583.

#### **FIGURES**

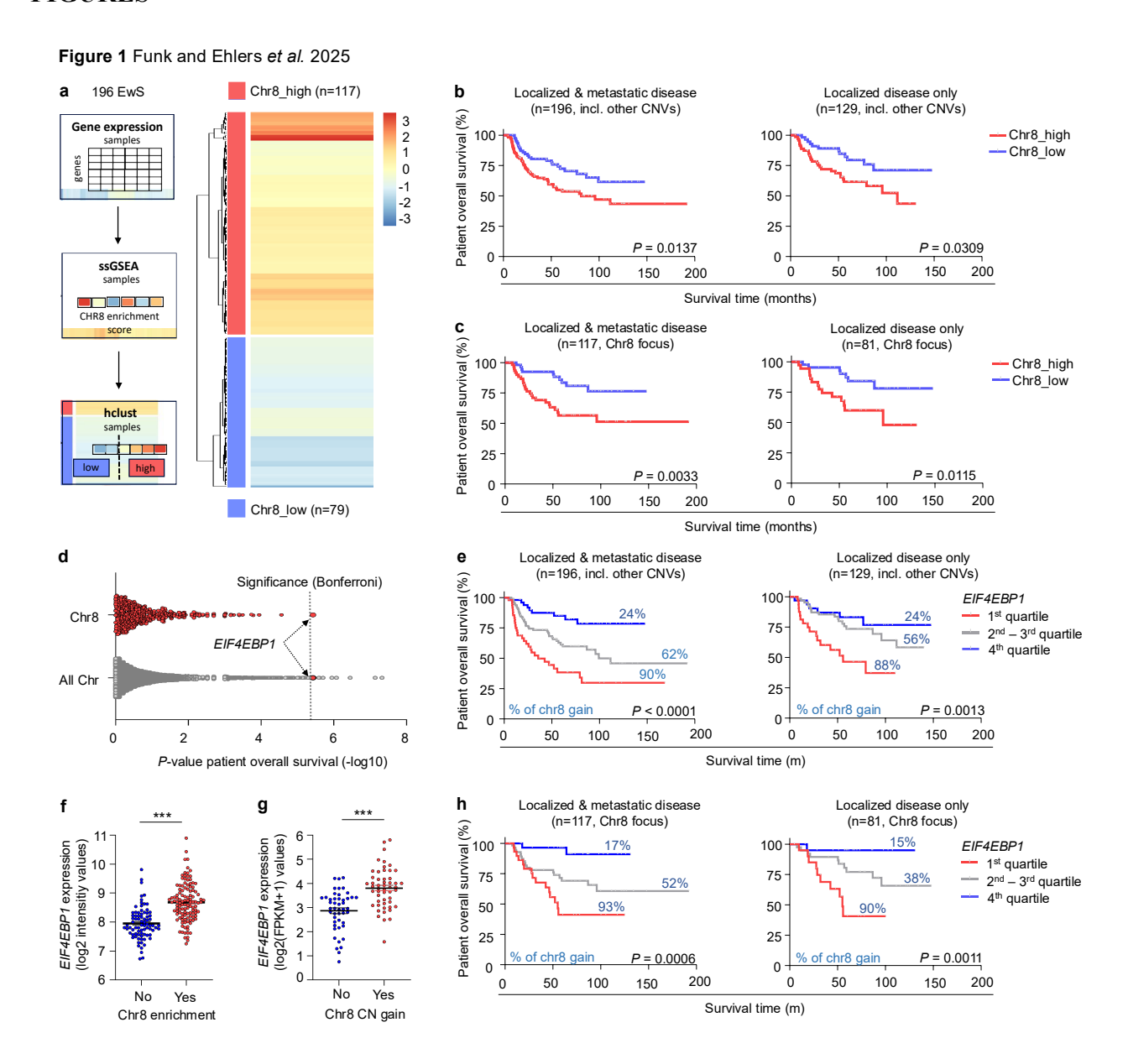


Figure 1: Chromosome 8 gain drives overexpression of the clinically relevant translation initiation factor 4E-BP1 in EwS.

- a Flowchart illustrating patient stratification to either a high or low chr8 gene expression signature group based on hierarchical clustering of sample-specific ssGSEA enrichment scores for the chromosome 8 gene set (left). Heat map of single-sample Gene Set Enrichment Analysis (ssGSEA) scores for chromosome 8 (chr8) genes in 196 EwS tumors (Cohort 1) (right). Hierarchical clustering identifies a chr8 high (n=117) and low (n=79) gene expression group. Color intensity indicates degree of gene set enrichment. Clustering method: median linkage, Euclidean distance on scaled enrichment scores.
- **b** Kaplan-Meier overall survival analysis of 196 EwS patients (Cohort 1) stratified into either a high or low chr8 signature enrichment group as described in (a). Kaplan-Meier plots are shown separately either for patients with localized & metastatic disease (n=196, left) or exclusively for patients with localized disease (n=129, right). *P*-values determined by Mantel-Haenszel test.
- c Kaplan-Meier overall survival analysis of 117 EwS patients (Cohort 1, Chr8 focus) stratified into either a high or low chr8 signature enrichment group as described in (a) but excluding samples with other inferred recurrent CNVs. Kaplan-Meier plots are shown separately either for patients with localized & metastatic disease (n=117, left) or exclusively for patients with localized disease (n=81, right). *P*-values determined by Mantel-Haenszel test.
- **d** Overall survival batch analysis as assessed for every gene covered in transcriptomic profiling of 196 EwS patients (Cohort 1) using Mantel-Haenszel statistics. Chr8-located genes were additionally depicted separately. The dashed line indicates the Bonferroni-adjusted *P*-value threshold for significance.

- e Kaplan-Meier overall survival analysis of 196 EwS patients (Cohort 1) stratified by quartile *EIF4EBP1* expression. Kaplan-Meier plots are shown separately either for patients with localized & metastatic disease (n=196, left) or exclusively patients with localized disease (n=129, right). Percentages given for each expression quartile refer to the percentage of patients showing predicted chr8 gain in the respective quartile. *P*-values determined by Mantel-Haenszel test
- **f** *EIF4EBP1* expression as measured by microarray profiling in 196 EwS patient tumors (Cohort 1) stratified into either a high or low chr8 signature enrichment group as described in (a). P-values determined by two-tailed Mann-Whitney test, horizontal bars represent means and whiskers represent the SEM. \*\*\*P<0.001.
- **g** *EIF4EBP1* expression as measured by RNA-seq in 100 EwS patient tumors (Cohort 2) depending on the presence of chr8 gain as determined by methylation array. P-values determined by two-tailed Mann-Whitney test, horizontal bars represent means and whiskers represent the SEM. \*\*\*P<0.001.
- **h** Kaplan-Meier overall survival analysis of 117 EwS patients (Cohort 1, Chr8 focus as in (c)) stratified by quartile *EIF4EBP1* expression. Kaplan-Meier plots are shown separately either for patients with localized & metastatic disease (n=117, left) or exclusively patients with localized disease (n=81, right). Percentages given for each expression quartile refer to the percentage of patients showing predicted chr8 gain in the respective quartile. *P*-values determined by Mantel-Haenszel test.

Figure 2 Funk and Ehlers et al. 2025

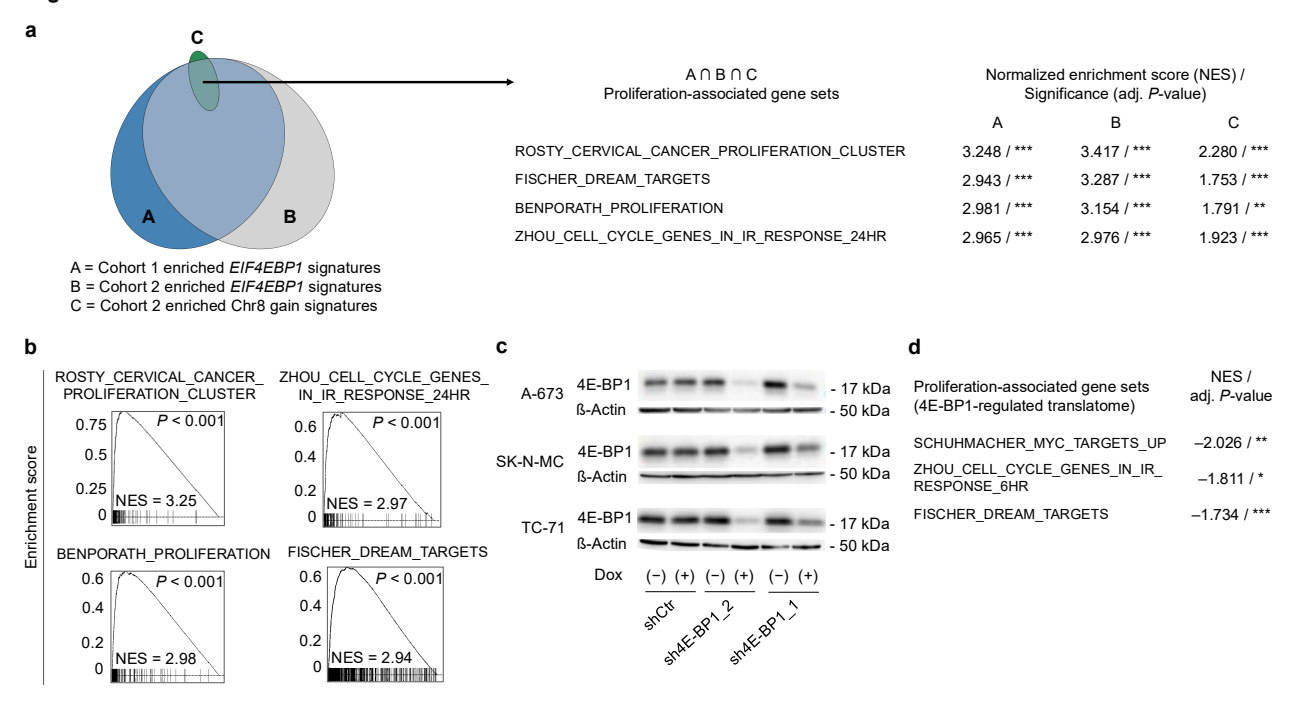


Figure 2: 4E-BP1 drives a proliferation-associated proteomic network.

a Area-proportional Venn diagram of gene sets enriched with EIF4EBP1 expression in Cohort 1 (A) and 2 (B) as well as with chr8 gain in Cohort 2 (C) as determined by fGSEA. Exemplary gene sets representing a proliferation-associated enrichment signature in the overlap between A, B, and C are shown with respective normalized enrichment scores (NES) and significance levels. \*\*\*P<0.001

**b** fGSEA enrichment plots of exemplary gene sets displayed in (a).

c Representative western blots in A-673, SK-N-MC, and TC-71 cells containing either Dox-inducible specific shRNA constructs directed against *EIF4EBP1* (sh4E-BP1\_1 or sh4E-BP1\_2) or a non-targeting shControl (shCtr). Cells were grown either with or without Dox for 96 h. β-Actin served as a loading control.

**d** Gene sets negatively enriched upon 4E-BP1 knockdown on protein level, as determined by fGSEA using integrated mass spectrometry and microarray protein/gene expression data as an input. Exemplary gene sets representing a proliferation-associated enrichment signature are shown with respective normalized enrichment scores (NES) and significance levels (\*\*\*P<0.001, \*\*P<0.01, \*P<0.05).

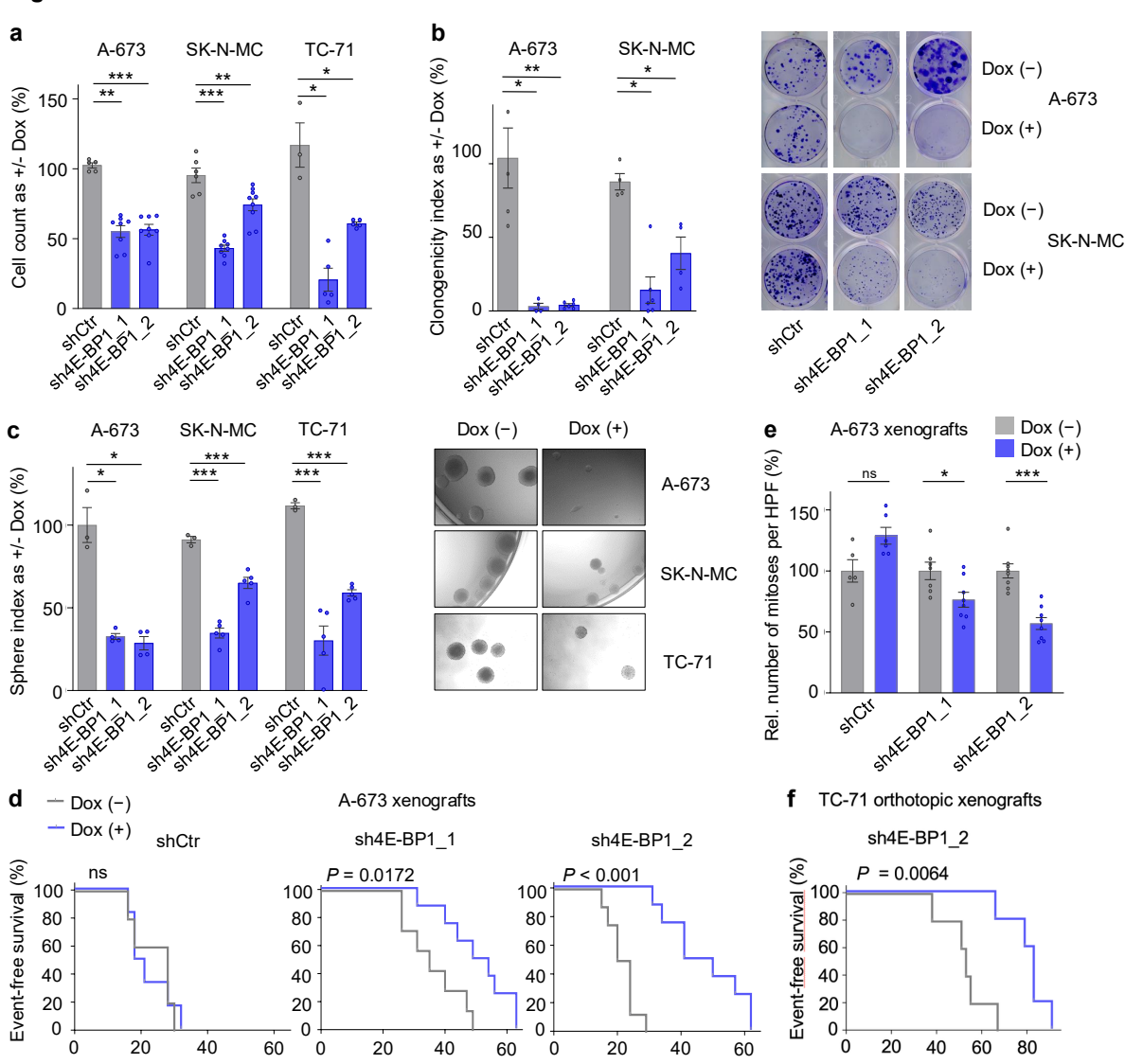


Figure 3 Funk and Ehlers et al. 2025

Figure 3: RNAi-mediated knockdown of 4E-BP1 inhibits EwS growth.

a Relative viable cell count of A-673, SK-N-MC, and TC-71 cells containing either Dox-inducible specific shRNA constructs directed against *EIF4EBP1* (sh4E-BP1\_1 or sh4E-BP1\_2) or a non-targeting shControl (shCtr) as measured by Trypan blue exclusion. Cells were grown either with or without Dox for 120 h. Horizontal bars represent means, and whiskers represent the SEM, n≥4 biologically independent experiments. *P*-values determined via one-tailed Mann-Whitney test and adjusted for multiple comparisons with the Benjamini-Hochberg method.

Event-free survival time (d)

- **b** Relative colony number of A-673 and SK-N-MC cells containing either Dox-inducible specific shRNA constructs directed against *EIF4EBP1* (sh4E-BP1\_1 or sh4E-BP1\_2) or a non-targeting shControl (shCtr). Cells were grown either with or without Dox for 8–14 d. Horizontal bars represent means, and whiskers the SEM, n≥4 biologically independent experiments. *P*-values determined via two-tailed Mann-Whitney test and adjusted for multiple comparisons with the Benjamini-Hochberg method. Representative images of colony formation are shown on the right.
- **c** Sphere formation in A-673, SK-N-MC, and TC-71 cells containing shRNA constructs directed against *EIF4EBP1* (sh4E-BP1\_1 or sh4E-BP1\_2) or a non-targeting shControl (shCtr) treated with or without Dox for 8–14 d. Horizontal bars represent means, and whiskers represent the SEM, n≥3 biologically independent experiments. *P*-values determined by two-tailed unpaired t-test with Welch's correction and adjusted for multiple comparisons with the Benjamini-Hochberg method. Representative images of spheres are shown on the right.
- **d** Kaplan-Meier analysis of event-free survival of NSG mice xenografted with A-673 cells containing either Doxinducible specific shRNA constructs directed against *EIF4EBP1* (sh4E-BP1\_1 or sh4E-BP1\_2) or a non-targeting shControl (shCtr). Once tumors were palpable, mice were randomized and treated with either vehicle (−) or Dox (+), n≥5 animals per condition. An 'event' was recorded when tumors reached a size maximum of 15 mm in one dimension. *P*-values determined via Mantel-Haenszel test.

e Quantification of mitoses in HE-stained slides of xenografts described in (d). Five high-power fields (HPF) were counted per sample. Horizontal bars represent means, and whiskers represent the SEM,  $n\ge4$  samples per condition. f Kaplan-Meier analysis of event-free survival of NSG mice orthotopically xenografted into the proximal tibia with TC-71 cells containing a Dox-inducible specific shRNA construct directed against EIF4EBP1 (sh4E-BP1\_2). One day after injection of the cells, mice were randomized and treated with either vehicle (–) or Dox (+), n=5 animals per condition. An 'event' is recorded when the mice exhibited signs of limping at the injected leg. P-values determined via Mantel-Haenszel test. \*\*\*P<0.001, \*\*P<0.01, \*P<0.05, ns = not significant; P-values determined via two-tailed Mann-Whitney test if not otherwise specified.

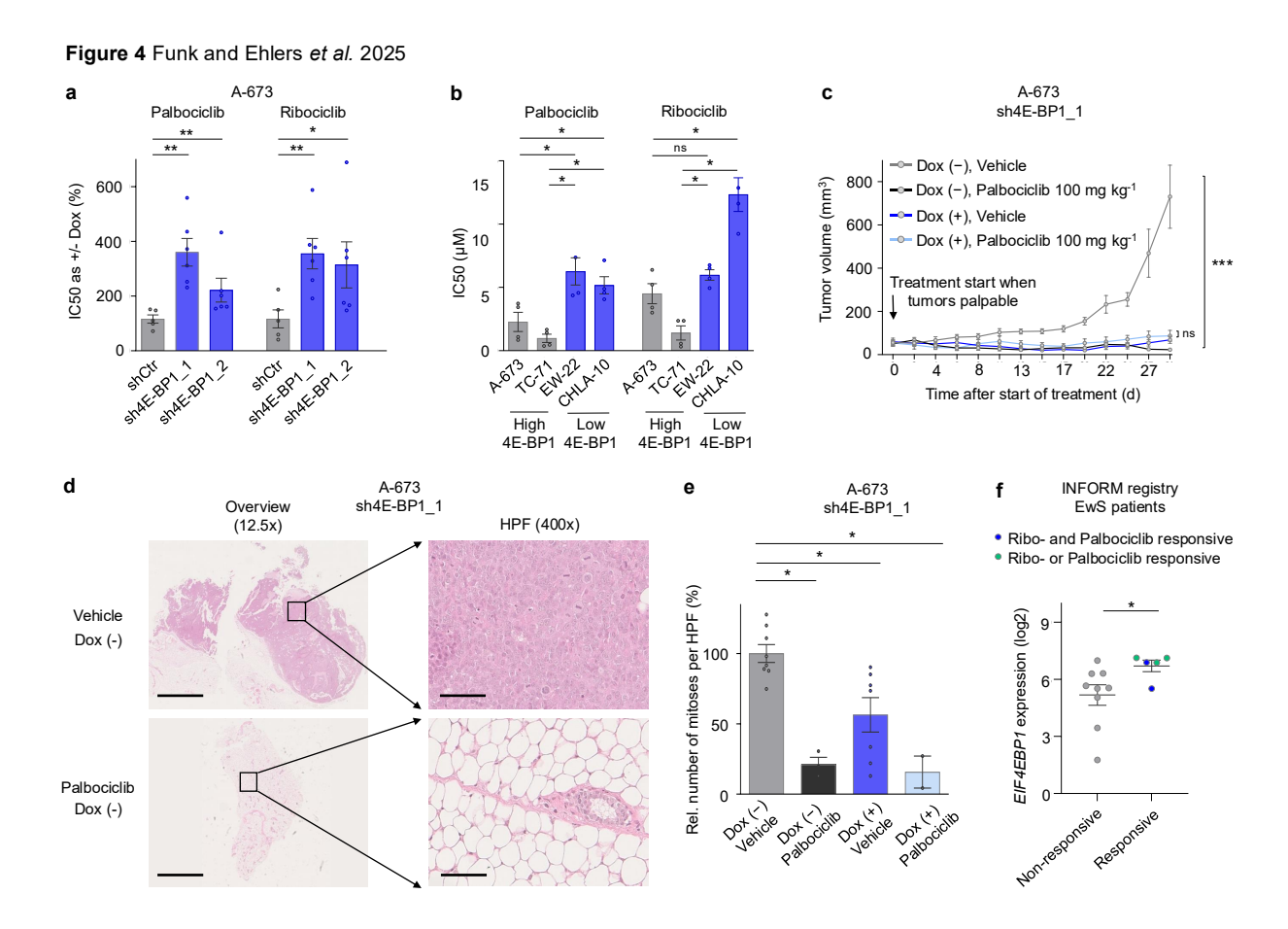


Figure 4: High 4E-BP1 expression sensitizes to targeted CDK4/6 inhibitor treatment with Palbociclib and Ribociclib.

a IC50 analysis of CDK4/6 inhibitors Palbociclib and Ribociclib in A-673 cells containing either DOX-inducible specific shRNAs directed against 4E-BP1 (sh4E-BP1\_1, sh4E-BP1\_2) or a non-targeting a non-targeting shControl (shCtr) as measured by resazurin colorimetry. Cells were treated with/without Dox as well as with serial dilutions of respective inhibitors. Horizontal bars represent means, and whiskers represent the SEM,  $n \ge 5$  biologically independent experiments. P-values determined via one-tailed Mann-Whitney test and adjusted for multiple comparisons with the Benjamini-Hochberg method.

**b** IC50 analysis of CDK4/6 inhibitors Palbociclib and Ribociclib in EwS cells with high (A-673, TC-71) and low (EW-22, CHLA-10) endogenous 4E-BP1 expression as measured by resazurin colorimetry. Cells were treated with serial dilutions of respective inhibitors. Horizontal bars represent means, and whiskers represent the SEM, n≥3 biologically independent experiments. *P*-values determined via one-tailed Mann-Whitney test and adjusted for multiple comparisons with the Benjamini-Hochberg method.

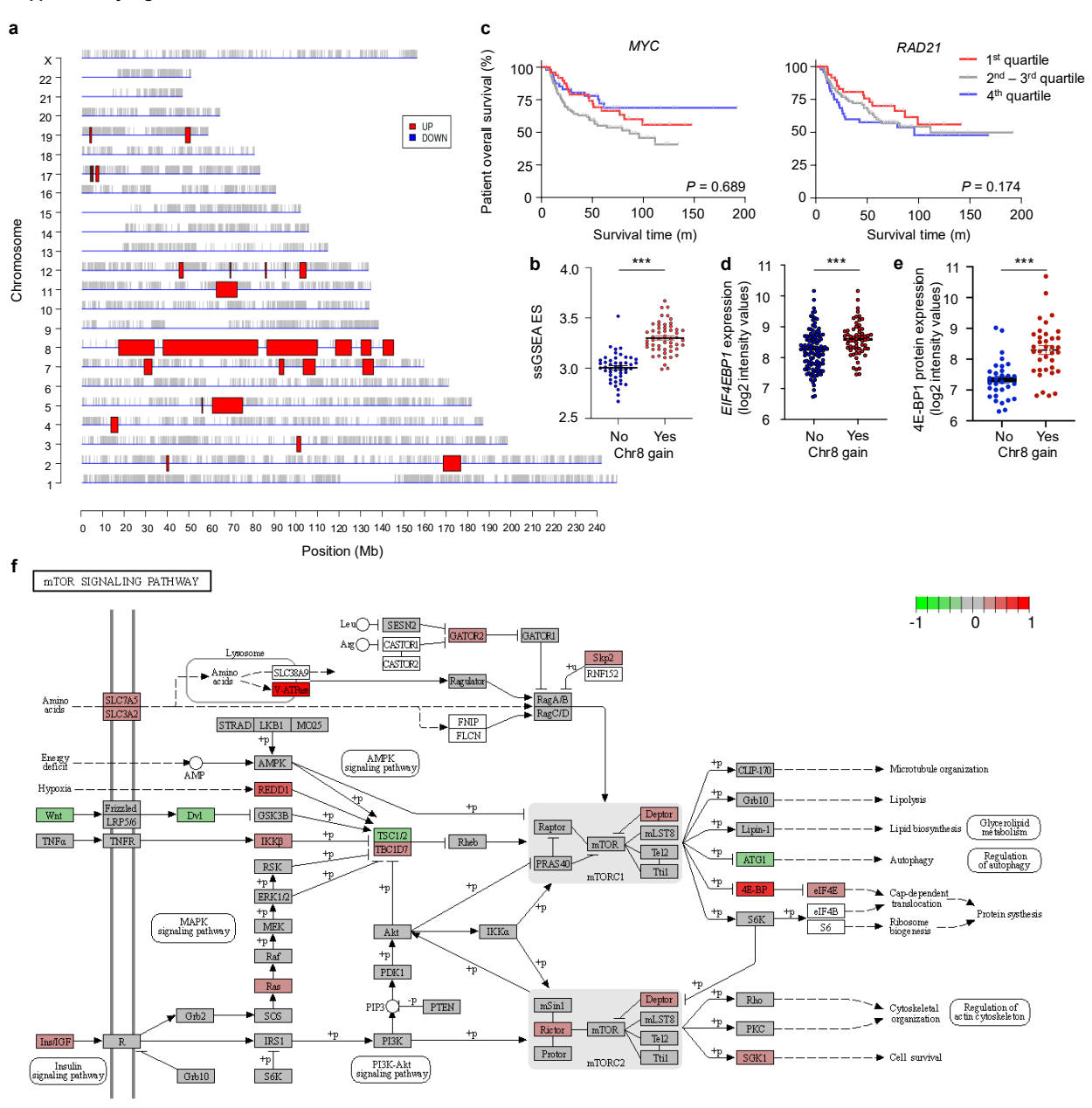
c NSG mice xenografted with A-673 EwS cells containing a Dox-inducible sh4E-BP1 construct, treated with/without Dox and either vehicle or Palbociclib in a dose of 100 mg/kg. Mice were randomized to the treatment groups when tumors were palpable. For each condition the mean tumor volume and SEM of 4–6 mice over the time of treatment are shown. *P*-values determined via two-tailed Mann-Whitney test and adjusted for multiple comparisons with the Benjamini-Hochberg method.

**d** Representative HE stained micrographs of A673/sh4E-BP1 xenografts (Dox (–)) treated with either vehicle or Palbociclib as described in (c) (shown as an overview with  $12.5 \times$  magnification and as a high-power field (HPF) in  $400 \times$  magnification). Scale bar is 2.5 mm ( $12.5 \times$ ) and  $100 \,\mu\text{m}$  ( $400 \times$ ).

e Quantification of mitoses in micrographs of xenografts described in (c). Horizontal bars represent means, and whiskers represent the SEM, n≥2 samples per condition. *P*-values determined via two-tailed Mann-Whitney test and adjusted for multiple comparisons with the Benjamini-Hochberg method.

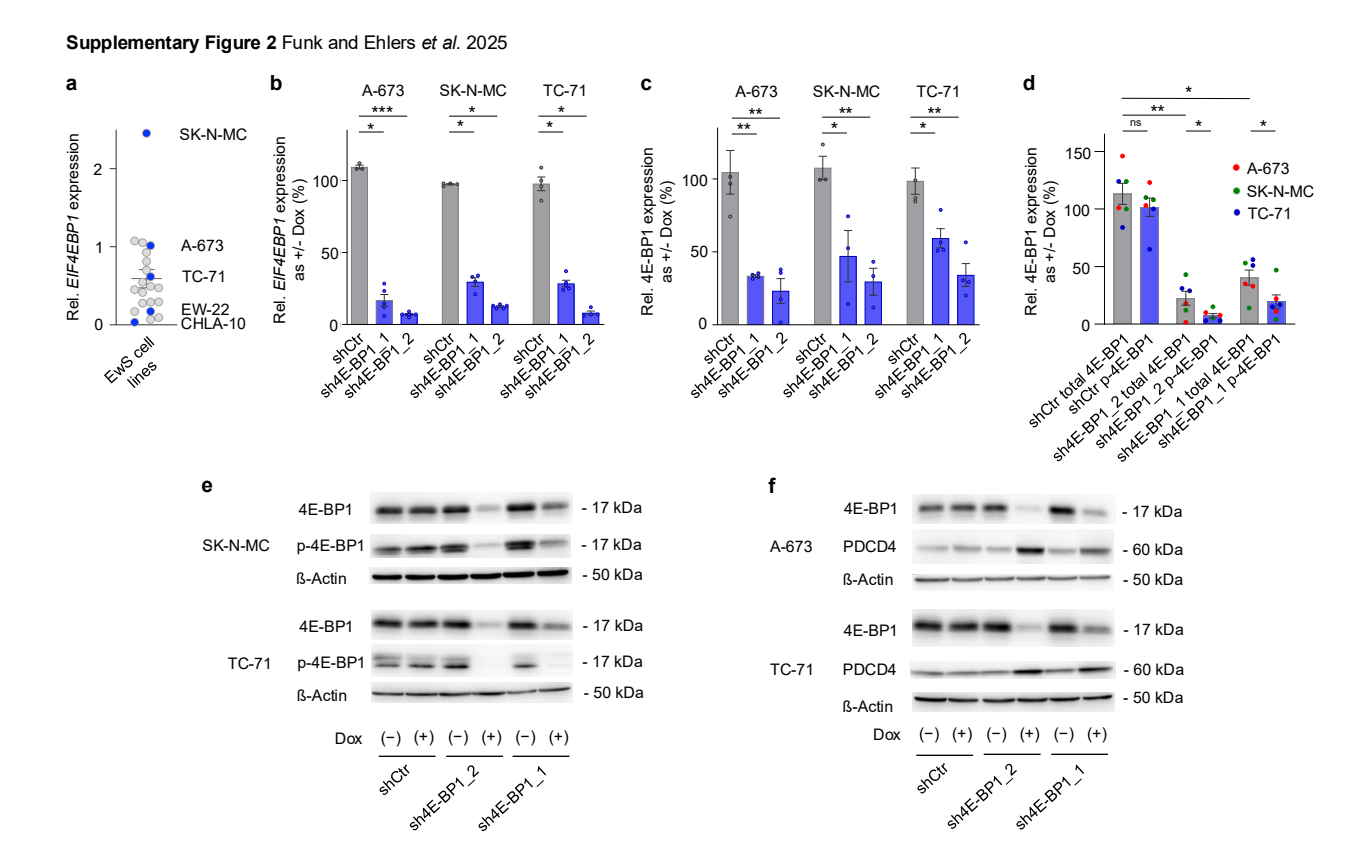
**f** *EIF4EBP1* gene expression data from 14 EwS patient tumors treated within the INFORM registry stratified according to matched Palbociclib/Ribociclib drug sensitivity data from 3D tumor cell cultures into a CDK4/6 inhibitor non-responsive and responsive group. \*\*\*P < 0.001, \*\*P < 0.01, \*\*P < 0.05, ns = not significant; P-values determined via two-tailed Mann-Whitney test if not otherwise specified.

#### Supplementary Figure 1 Funk and Ehlers et al. 2025



### Supplementary Figure 1: Model validation, chromosomal location, and mTOR pathway representation of genes differentially upregulated in the chr8 high gene expression signature group in EwS.

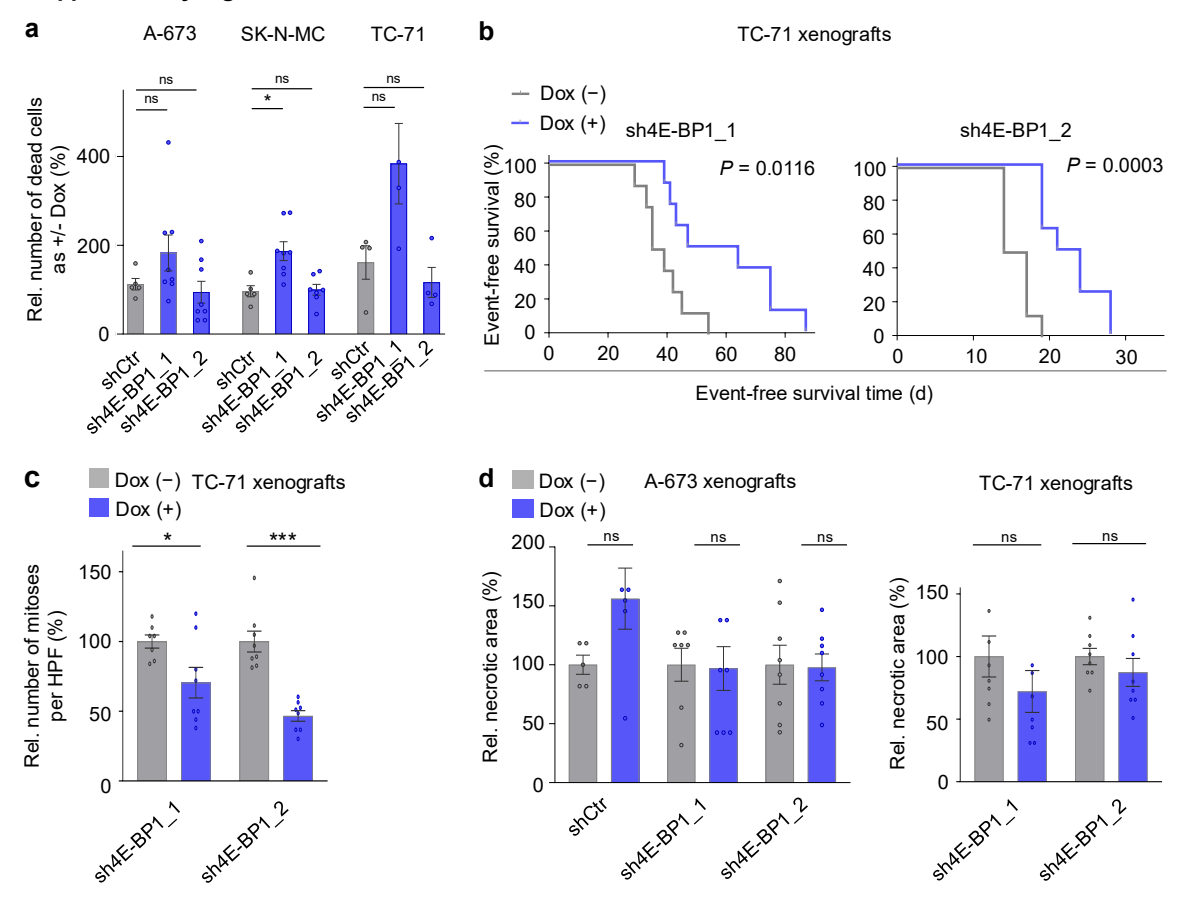
- **a** Differentially expressed genes (DEGs) between the chr8 high and low gene enrichment clusters mapped onto chromosome positions using Position Related Data Analysis (PREDA).
- **b** ssGSEA enrichment scores for chr8 gene expression enrichment as measured by RNA-seq in 100 primary EwS (Cohort 2) depending on the presence of factual chr8 gain as determined by methylation array.
- **c** Kaplan-Meier overall survival analysis of 196 EwS patients (Cohort 1) stratified by quartile *MYC* or RAD21 expression. *P*-values determined by Mantel-Haenszel test.
- **d** *EIF4EBP1* expression as measured by microarray profiling in 117 EwS patients (Cohort 1, Chr8 focus) stratified into either a high or low chr8 signature enrichment group as shown in (Figure 1e) but excluding samples with other inferred recurrent CNVs. *P*-values determined by two-tailed Mann-Whitney test, horizontal bars represent means and whiskers represent the SEM.
- **e** 4E-BP1 protein expression as measured by mass spectrometry in a subset of Cohort 2 for which 4E-BP1 protein expression data were available. 4E-BP1 expression is shown depending on the evidence of chr8 gain in methylation array data. *P*-values determined by two-tailed Mann-Whitney test, horizontal bars represent means and whiskers represent the SEM.
- **f** DEGs between the chr8 high and low gene expression cluster in Cohort 1 within the mTOR signaling pathway. \*\*\*P < 0.001, P-values determined via two-tailed Mann-Whitney test.



#### Supplementary Figure 2: 4E-BP1 drives a proliferation-associated proteomic network.

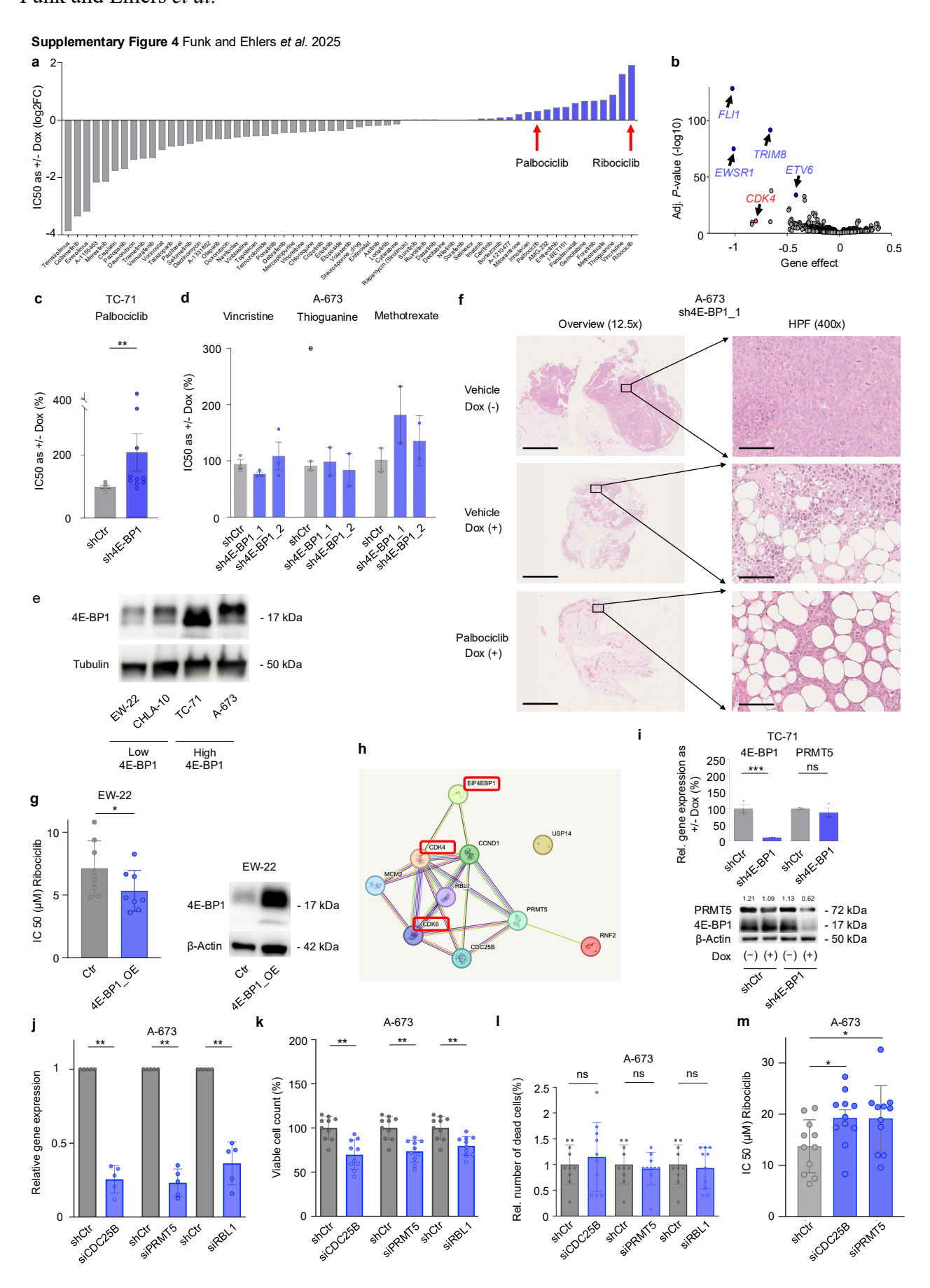
- a Relative *EIF4EBP1* expression in 21 wildtype EwS cell lines as determined by qRT-PCR. *EIF4EBP1* expression of each cell line is normalized to that of A-673.
- **b** Relative *EIF4EBP1* expression as assessed by qRT-PCR in A-673, SK-N-MC, and TC-71 cells containing either Doxinducible specific shRNA constructs directed against *EIF4EBP1* (sh4E-BP1\_1 or sh4E-BP1\_2) or a non-targeting shControl (shCtr). Cells were grown either with or without Dox for 96 h. Horizontal bars represent means, and whiskers represent the SEM, n≥3 biologically independent experiments. *P*-values determined via two-tailed Mann-Whitney test and adjusted for multiple comparisons with the Benjamini-Hochberg method.
- **c** Relative 4E-BP1 expression as assessed by quantified western blotting in A-673, SK-N-MC, and TC-71 cells containing either Dox-inducible specific shRNA constructs directed against *EIF4EBP1* (sh4E-BP1\_1 or sh4E-BP1\_2) or a non-targeting shControl (shCtr). Cells were grown either with or without Dox for 96 h. *P*-values determined via unpaired t-test and adjusted for multiple comparisons with the Benjamini-Hochberg method.
- **d** Relative total and phospho (Ser65) 4E-BP1 expression as assessed by quantified western blotting in A-673, SK-N-MC, and TC-71 cells containing either Dox-inducible specific shRNA constructs directed against *EIF4EBP1* (sh4E-BP1\_1 or sh4E-BP1\_2) or a non-targeting shControl (shCtr). Cells were grown either with or without Dox for 96 h. *P*-values determined via one-tailed Mann-Whitney test and adjusted for multiple comparisons with the Benjamini-Hochberg method.
- e Representative western blots in SK-N-MC and TC-71 cells of experiments described in (d). β-Actin served as a loading control.
- f Representative western blots showing total 4E-BP1 and PDCD4 expression levels in A-673 and TC-71 cells containing either Dox-inducible specific shRNA constructs directed against *EIF4EBP1* (sh4E-BP1\_1 or sh4E-BP1\_2) or a nontargeting shControl (shCtr). Cells were grown either with or without Dox for 96 h. β-Actin served as a loading control.

#### Supplementary Figure 3 Funk and Ehlers et al. 2025



#### Supplementary Figure 3: RNAi-mediated knockdown of 4E-BP1 inhibits EwS growth.

- a Relative number of dead cells as assessed by Trypan blue exclusion in A-673, SK-N-MC, and TC-71 cells containing either Dox-inducible specific shRNA constructs directed against *EIF4EBP1* (sh4E-BP1\_1 or sh4E-BP1\_2) or a nontargeting shControl (shCtr). Cells were grown either with or without Dox for 96 h. Horizontal bars represent means, and whiskers represent the SEM, n≥4 biologically independent experiments. *P*-values determined via two-tailed Mann-Whitney test and adjusted for multiple comparisons with the Benjamini-Hochberg method.
- **b** Kaplan-Meier analysis of event-free survival of NSG mice xenografted with TC-71 cells containing Dox-inducible specific shRNA constructs directed against *EIF4EBP1* (sh4E-BP1\_1 or sh4E-BP1\_2). Once tumors were palpable, mice were randomized and treated with either vehicle (–) or Dox (+), n=8 animals per condition. An 'event' was recorded when tumors reached a size maximum of 15 mm in one dimension. *P*-values determined via Mantel-Haenszel test.
- c Quantification of mitoses in HE-stained slides of xenografts described in (b). Five high-power fields (HPF) were counted per sample. Horizontal bars represent means, and whiskers represent the SEM,  $n \ge 7$  samples per condition.
- d Quantification of necrotic area on HE-stained slides of A-673 and TC-71 xenografts described in (Fig. 3d, Suppl. Fig. 3b). Five high-power fields (HPF) were analyzed per sample. Horizontal bars represent means, and whiskers represent the SEM, n≥5 samples per condition.



Supplementary Figure 4: High 4E-BP1 expression sensitizes for targeted CDK4/6 inhibitor treatment with Palbociclib and Ribociclib.

**a** IC50 analysis of 3D culture drug screening data of A-673 EwS cells containing a Dox-inducible shRNA directed against 4E-BP1 and treated with/without Dox and respective indicated inhibitors in serially increasing concentrations.

- **b** Volcano plot showing gene dependency effects of indicated genes in EwS cell lines as compared to all non-EwS cell lines with respective individual statistical significance values (-log10 adj. *P*-value).
- c IC50 analysis of CDK4/6 inhibitor Palbociclib in TC-71 cells containing either DOX-inducible specific shRNAs directed against 4E-BP1, or a non-targeting a non-targeting shControl (shCtr) as measured by resazurin colorimetry. Cells were treated with/without Dox as well as with serial dilutions of the inhibitors. Horizontal bars represent means, and whiskers represent the SEM,  $n \ge 5$  biologically independent experiments.
- **d** IC50 analysis of Vincristine, Thioguanine, and Methotrexate in A-673 cells containing either DOX-inducible specific shRNAs directed against 4E-BP1 (sh4E-BP1\_1, sh4E-BP1\_2) or a non-targeting a non-targeting shControl (shCtr) as measured by resazurin colorimetry. Cells were treated with/without Dox as well as with serial dilutions of respective drugs. Horizontal bars represent means, and whiskers represent the SEM,  $n \ge 2$  biologically independent experiments.
- **e** Representative western blots in EW-22, CHLA-10 (low 4E-BP1 expressing) and TC-71 and A-673 (high 4E-BP1 expressing) EwS cells. β-Actin served as a loading control.
- f IC50 analysis of Ribociclib in EW-22 cells containing either a 4E-BP1 overexpression construct (4E-BP1\_OE) or a negative control (Ctr) construct as measured by resazurin colorimetry (left). Cells were treated with a serial dilution of Ribociclib. Horizontal bars represent means, and whiskers represent the SEM, n=8 biologically independent experiments. Representative western blots in EW-22 cells containing either a 4E-BP1 overexpression construct (4E-BP1\_OE) or a negative control (Ctr) construct (right). β-Actin served as a loading control.
- g Representative HE stained micrographs of A673/sh4E-BP1 xenografts (Dox (-) / Dox (+)) treated with either vehicle or Palbociclib as described in (Figure 4c) (shown as an overview with  $12.5 \times$  magnification and as a high-power field (HPF) in  $400 \times$  magnification). Scale bar is 2.5 mm ( $12.5 \times$ ) and  $100 \text{ }\mu\text{m}$  ( $400 \times$ ).
- **h** STRING interaction analysis of the following proteins: EIF4EBP1, CDK4, CDK6, CCND1, CDC25B, PRMT5, MCM2, RBL1, RNF2, and USP14. Color codes of lines and nodes indicate form of interaction as defined by the STRING database. EIF4EBP1 and CDK4/6 are highlighted in red rectangles.
- i Upper panel: Relative *EIF4EBP1* and *PRMT5* expression as assessed by qRT-PCR in TC-71 cells containing either Dox-inducible specific shRNA constructs directed against *EIF4EBP1* (sh4E-BP1) or a non-targeting shControl (shCtr). Cells were grown either with or without Dox for 96 h. Horizontal bars represent means, and whiskers represent the SEM, n=3 biologically independent experiments. Lower panel: Representative corresponding western blots of the same experiments using antibodies against 4E-BP1 and PRMT5. Numbers indicate the densitometry ratios of PRMT5 normalized to β-Actin. β-Actin served as a loading control.
- **j** Relative expression of *CDC25B*, *PRMT5*, and *RBL1* as assessed by qRT-PCR in A-673 cells treated either with siPools directed against respective genes or a negative control siPool. Horizontal bars represent means, and whiskers represent the SEM, n=5 biologically independent experiments.
- **k** Relative viable cell count of A-673 cells treated either with siPools directed against *CDC25B*, *PRMT5*, or *RBL1*, or a negative control siPools as measured by Trypan blue exclusion. Cells were assayed 120 h after knockdown induction. Horizontal bars represent means, and whiskers represent the SEM, n=10 biologically independent experiments.
- I Relative number of dead cells in experiments detailed in (i) as measured by Trypan blue exclusion. Horizontal bars represent means, and whiskers represent the SEM, n=10 biologically independent experiments. *P*-values determined via two-tailed Mann-Whitney test and adjusted for multiple comparisons with the Benjamini-Hochberg method.
- m IC50 analysis of Ribociclib in A-673 cells treated either with siPools directed against *CDC25B* or *PRMT5*, or a negative control siPool as measured by resazurin colorimetry. Cells were additionally treated with a serial dilution of Ribociclib. Horizontal bars represent means, and whiskers represent the SEM, n=11 biologically independent experiments.
- \*\*\*P < 0.001, \*\*P < 0.05, ns = not significant; P-values determined via two-tailed Mann-Whitney test if not otherwise specified.